https://doi.org/10.5194/egusphere-2026-1345
Preprint. Discussion started: 18 March 2026

Automated Avalanche Hazard Indication for Southeast Alaska

Elizabeth Fischer[1], Gabriel J. Wolken[2], Yves Bühler[34], Marc Christen[5], and Rick Lader[1]

[1]University of Alaska, Fairbanks, USA
[2]Alaska Division of Geological & Geophysical Surveys
[3]WSL Institute for Snow and Avalanche Research SLF, Davos, Switzerland
[4]Climate Change, Extremes and Natural Hazards in Alpine Regions Research Centre (CERC), Davos, Switzerland
[5]RAMMS AG, Davos, Switzerland

Correspondence: Elizabeth Fischer (eafischer2@alaska.edu)

Abstract. Snow avalanches represent a significant yet poorly characterized natural hazard in Alaska, where risk assessment is limited by extreme data scarcity, rapidly changing climate conditions, and land-use policies that often inadequately account for environmental uncertainty. We address these challenges in Southeast Alaska by developing the region's first systematic, large-scale avalanche hazard indication maps to support public safety, infrastructure planning, and land-use decision-making. To overcome sparse observational records, we developed a hybrid modeling framework that integrates downscaled reanalysis for historical baselines (1981–2010) with dynamically downscaled climate projections for mid-century conditions (2031-–2060). More than 3.5 million avalanche simulations were performed using RAMMS::LSHIM driven by downscaled snow inputs. Forest landcover masks were incorporated to represent both suppression of avalanche release and vegetation-induced braking during runout, recognizing that these simplified effects remain sensitive to landcover classification accuracy and assumed release-area configurations. The resulting maps reveal a heterogeneous response of avalanche hazards to climate change. At lower elevations, hazard extents generally decrease as warming temperatures shift precipitation from snow to rain. In contrast, select high-elevation areas of northern Southeast Alaska are projected to experience increased runout, where persistently low temperatures, combined with enhanced atmospheric moisture, lead to greater maximum snowfall. Collectively, these results provide the first region-wide, climate-informed assessment of avalanche susceptibility in Southeast Alaska, establishing a critical foundation for hazard adaptation, infrastructure resilience, and future mitigation strategies across Alaska's sub-Arctic landscapes.

1 Introduction

Hazard maps are a key tool to cope with avalanche hazard in settled regions within alpine terrain (Boensch et al., 2014; Rudolf-Miklau et al., 2014). They are generated by avalanche experts for individual avalanche tracks by combining historical records, field investigations, terrain analysis, forest information, snow climatology and numerical modeling; and they have proven to be an effective and reliable tool to prevent avalanche damage and victims (Margreth and Romang, 2010). However, avalanche hazard mapping in Alaska is restricted to selected areas, typically those with existing infrastructure. This is due to the lack of

https://doi.org/10.5194/egusphere-2026-1345
Preprint. Discussion started: 18 March 2026

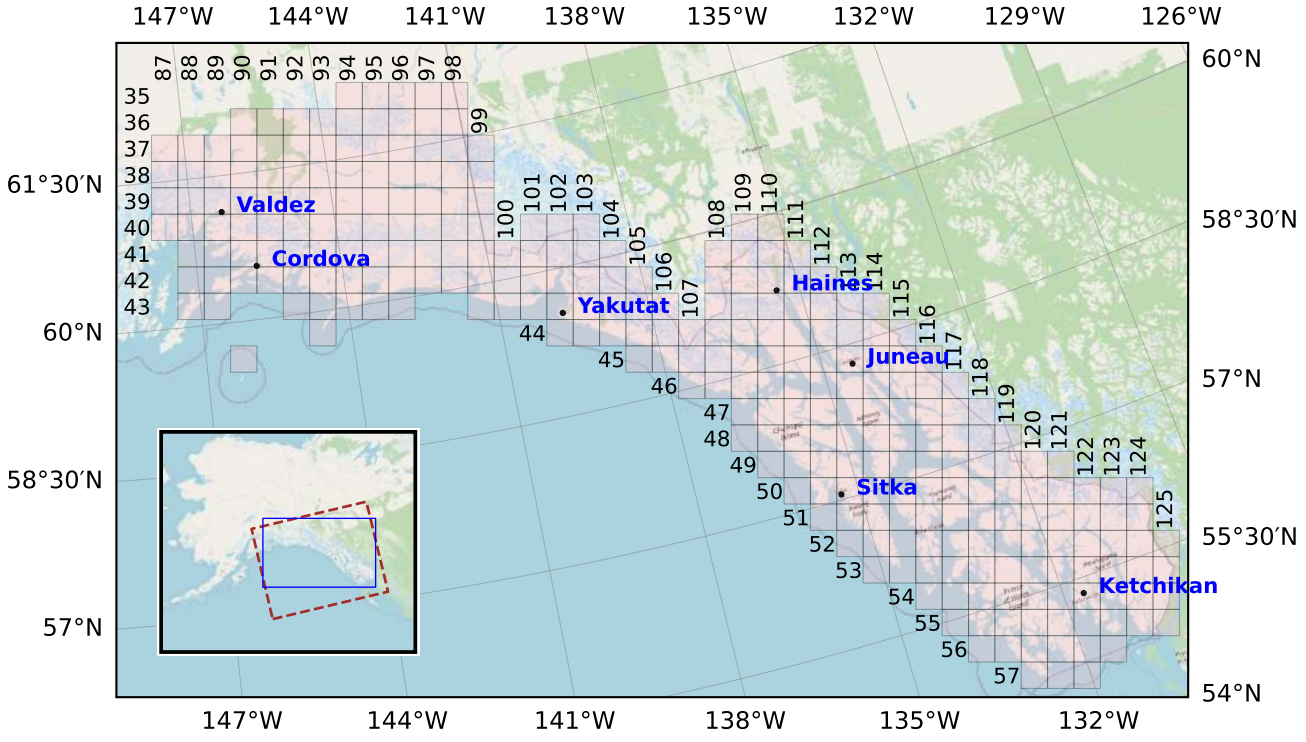

Figure 1. Reference map showing the $30\,\mathrm{km}$ square *tiles* used to divide the Southeast Alaska domain into computationally manageable pieces. Numbers across the top and down the left side of the domain show the i and j coordinates, respectively, of each tile, with the city of Juneau has coordinates $(113, 45)$. **Inset Map:** The dotted red outline shows the WRF computational domain, and the blue square locates the domain of the main map.

both in situ meteorological and avalanche observations across the majority of the sparsely populated state, and to the high cost of map creation.

Complementing detailed avalanche hazard maps, hazard indication maps (Bühler et al., 2022; Issler et al., 2023) are designed for rapid large-scale assessments, providing a broad overview of potential avalanche hazard. They are less detailed than hazard maps, and they use automated systems and readily available data to identify areas of increased avalanche hazard. Although early attempts were made to understand avalanche risk in Alaska qualitatively (Hackett and Santeford, 1980), it was not until 2022 that Bühler et al. (2022) developed a reliable and carefully validated algorithm to delineate potential avalanche release areas (PRAs) (Maggioni and Gruber, 2003; Bühler et al., 2013), enabling the application of the state-of-the-art avalanche dynamics model Rapid Mass Movement Simulation (RAMMS::LSHIM) (Christen et al., 2010) to automatically generate hazard indication maps on a large scale (Bühler, 2018) and to produce terrain classifications for backcountry touring (Harvey et al., 2018). Bühler et al. (2022) applied this methodology to the Canton of Grisons in Switzerland, delineating and simulating over 3 million avalanches over a total area of $7105\,\mathrm{km}^2$.

https://doi.org/10.5194/egusphere-2026-1345
Preprint. Discussion started: 18 March 2026

While detailed avalanche hazard maps exist for limited areas in Southeast Alaska, such as the region around Juneau (WSL Institute, 2011; TetraTech, 2022), the vast majority of the state remains unmapped, presenting a significant challenge for assessing risk to people, infrastructure, ecosystems, and access to natural resources. Southeast Alaska is characterized by its large size ($91{,}000\,\mathrm{km}^2$ extending $800\,\mathrm{km}$ along the coast), steep glacially carved terrain with numerous fjords, and lack of road network, and there is a critical dearth of well-distributed meteorological data. Weather stations are sparse, particularly at elevations relevant to avalanche initiation zones, and those that exist often possess short observational records. To address this data scarcity and provide a foundational understanding of avalanche hazard potential, we generate automated avalanche hazard indication maps for Southeast Alaska (Figure 1), adapting the methodology of Bühler et al. (2022) to account for the region's unique environmental factors and data limitations. We produce these maps for both a recent historic climatological period (1981–2010) and a future climatological scenario (2031–2060). To account for the spatial and temporal limitations of in-situ meteorological observations, we employ a hybrid approach: for the recent historical period, we derive climatological conditions from downscaled reanalysis, whereas for the future scenario we use dynamically downscaled climate model output. This strategy allows us to approximate the necessary meteorological inputs for large-scale modeling of avalanches in Southeast Alaska despite the challenging observational environment.

A crucial opportunity for validation exists where detailed avalanche hazard studies have been undertaken by local experts. These studies, such as those found in the Juneau area (WSL Institute, 2011; TetraTech, 2022), a city known to be at the highest risk in the U.S. for urban avalanches, provide existing observations of past events and in-situ weather. This existing body of work is essential for validating our automated approach and adding to our understanding of the hazards in this region. The remainder of this paper is structured as follows: Section 2 describes the data sets used and our adapted methodology, which closely follows Bühler et al. (2022); Section 3.1 compares our results to existing observational data and expert studies (WSL Institute, 2011; TetraTech, 2022; Fesler and Fredson, 2000); Section 3.2 summarizes wide area statistics of avalanche prevalence and how it is expected to change in the future; Section 3.3 offers discussion, conclusion and future directions; Section 3.4 dicsusses the imprecision in recurrence intervals that is inherent in this study; Section 3.5 reviews the lack of observational data and the limitations of our approach; and Section 4 provides final summary conclusions from this work.

2 Methods and Data

As described in Bühler et al. (2022), the development of avalanche hazard indication maps require three data sets: a digital elevation model, forest tree cover, and maximum 3-day daily snowfall. In this study we obtain those three components as follows. Automated hazard indication maps contain rough model-based estimates of the maximum hazard area affected in the case of an extreme event; however, they usually do not contain any information about the intensities that will occur, nor do they incorporate other variables pertinent to individual avalanche behavior, such as the rate of temperature change or the wind velocity. All data sets use the Alaska Albers projection, or EPSG:3338.

https://doi.org/10.5194/egusphere-2026-1345
Preprint. Discussion started: 18 March 2026

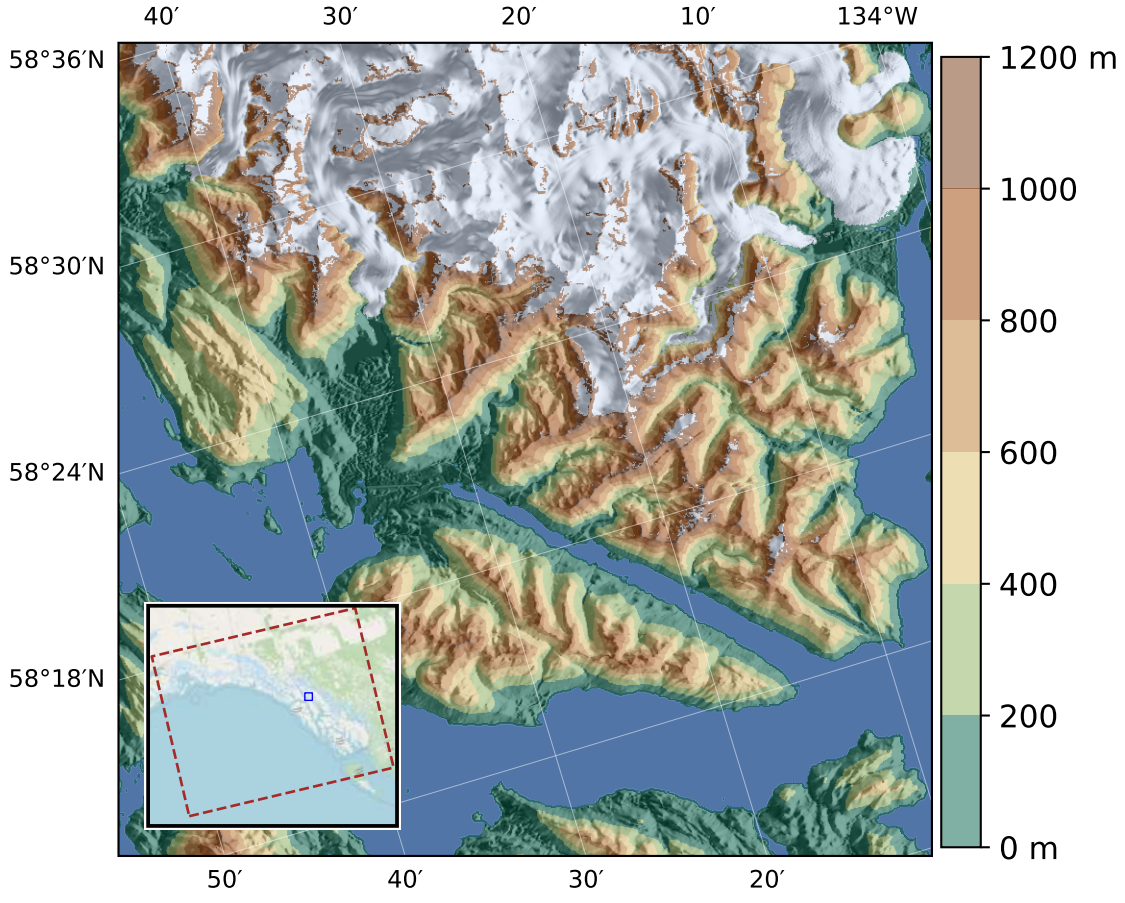

Figure 2. Elevation data from Juneau area (5 m resolution), with glaciers shown in white. **Inset Map:** The dotted red outline shows the WRF computational domain. The blue square locates the domain of the main map.

2.1 Elevation Data

We used the interferometric synthetic aperture radar (IFSAR) digital elevation dataset from the United States Geological Survey (Carswell Jr., 2013), providing 5 m resolution (Figure 2). To accommodate the smoothing effect of snow on terrain and to reduce the computational load during avalanche simulations, we resampled the elevation data to 10 m using the GDAL nearest neighbor subsampling (GDAL/OGR contributors, 2024).

2.2 Forest Data

Alpine forests can stabilize snowpack, hinder avalanche initiation and reduce avalanche flow in the runout zone (Viglietti et al., 2009). However large avalanches, once initiated, can destroy forests (Bartelt and Stöckli, 2001), leaving visible scars along avalanche tracks. Modeling the interactions between avalanche inhibition and forest destruction requires consideration

https://doi.org/10.5194/egusphere-2026-1345
Preprint. Discussion started: 18 March 2026

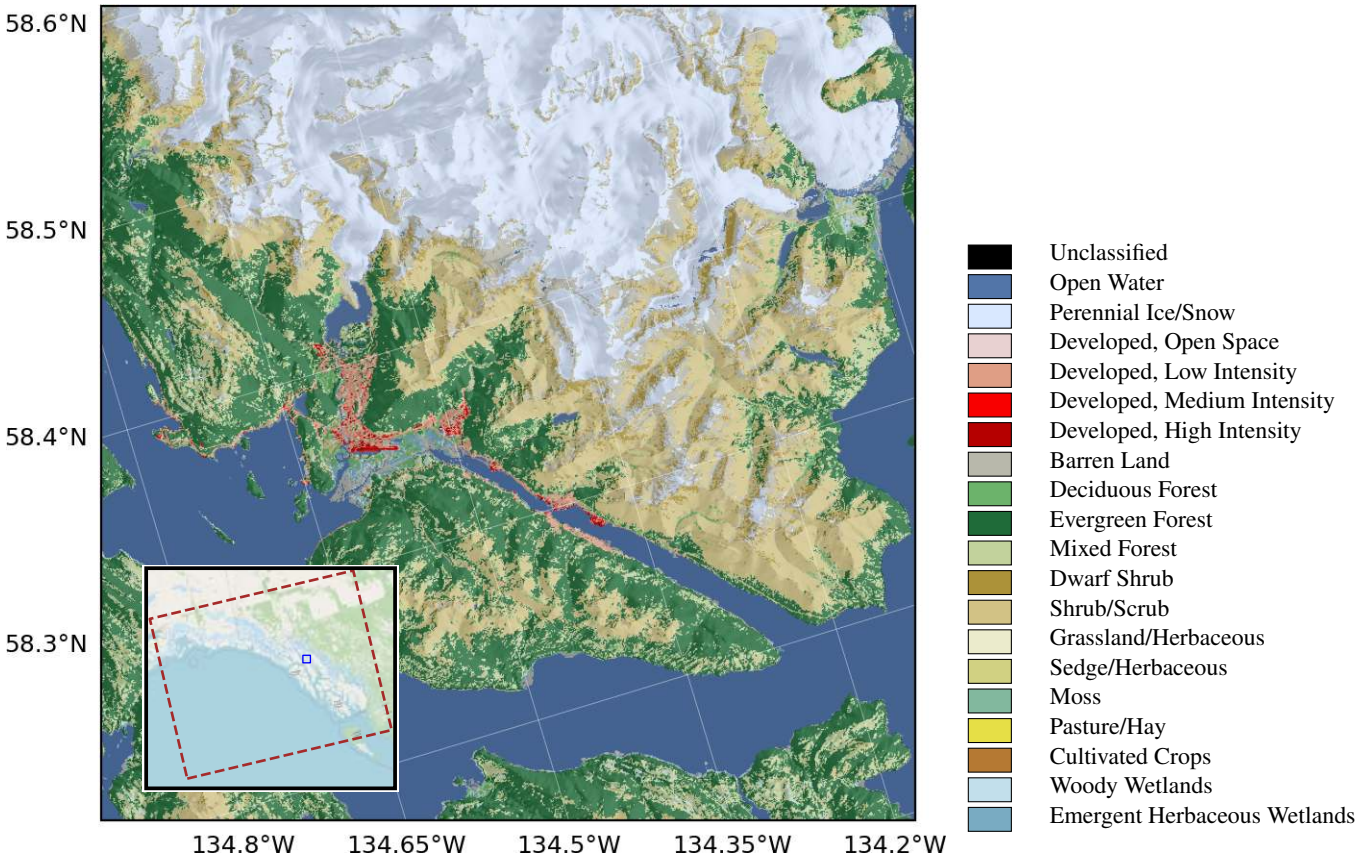

Figure 3. Land cover data from Juneau area, from the Alaska Land Cover Database 2016 (NLCD) (Jin et al., 2019). **Inset Map:** The dotted red outline shows the WRF computational domain. The blue square locates the domain of the main map.

of detailed tree characteristics, information that is not available in most of Alaska. RAMMS::LSHIM models these phenomena more simply using a *forest mask*, which labels each gridcell as *"non-forest"* or *"avalanche protection forest"* (Bebi et al., 2021; Bühler et al., 2022), and is not able to effect nuanced differences in vegetation between regions. The forest mask is used in the following ways:

1. PRAs are created to encompass only *non-forest* gridcells.
2. For the PRAs classified as *small* or *tiny* (PRA area of $25{,}000\,\mathrm{m}^2$ or less), the turbulent friction is set to $400\,\mathrm{m\,s}^{-1}$ in *avalanche protection forest* gridcells, thereby braking the velocity of the avalanche.
3. For PRAs classified as *medium* or *large* (PRA area of more than $25{,}000\,\mathrm{m}^2$), the forest mask is not used because such avalanches develop impact pressures that reach destructive forces ($> 500\,\mathrm{kPa}$) and are assumed to destroy forests in their path without significant braking effect.

https://doi.org/10.5194/egusphere-2026-1345
Preprint. Discussion started: 18 March 2026

We obtained a forest cover mask from the Alaska Land Cover Database 2016 (NLCD) (Jin et al., 2019), which is based on composites of Landsat imagery (Figure 3) and is the most advanced, spatially extensive land cover data available for Alaska at the time of writing. The finest resolution of this database is $30\,\mathrm{m}$, whereas our analysis with RAMMS::LSHIM uses $10\,\mathrm{m}$ resolution. Therefore, we resampled the NLCD data to $10\,\mathrm{m}$ using a nearest neighbor algorithm, effectively turning each original $30\,\mathrm{m}$ gridcell into a 3×3 block of $10\,\mathrm{m}$ gridcells. The relatively low resolution of the NCLD data makes it impossible to accurately map certain narrow avalanche tracks. Additionally, the NCLD database does not provide detailed vegetation information such as tree height, crown cover and gap width, which Bühler et al. (2022) used to compute the avalanche protection forest mask. Instead, we compute the forest mask by considering the forest-type classifications available in NCLD: *Deciduous Forest* (41), *Evergreen Forest* (42) and *Mixed Forest* (43):

- Evergreen forests in Southeast Alaska are dominated by large species such as *Western Hemlock* and *Sitka Spruce* (Védrine et al., 2022), which protect against avalanches. Therefore NCLD class 42 is included in the forest mask.
- Deciduous "forest" in Southeast Alaska is dominated by trees such as Alder species (Harris and Farr, 1974), with thin flexible stems that do little to stop the initiation or spread of avalanches. Alders are a successional species, most common in areas disturbed for example by large avalanches, logging or fire (Harris and Farr, 1974). Therefore, NCLD class 41 is *not* included in the forest mask.
- Areas classified as *Mixed Forest* are harder to characterize. We chose to *not* include them in the forest mask under the initial assumption that they do not offer significant avalanche protection. This results in more low elevation PRAs — those below the tree line — since most non-evergreen forest occurs at low elevations. This choice is appropriate since additional steps are taken to cull unrealistic low elevation avalanches (Section 2.11). Note that most avalanche hazard occurs from PRAs initiating avalanches above the tree line, where they can develop long runout paths, high velocities and destructive forces.

The NCLD data misclassify some areas, which in some cases can be detected manually through knowledge of the local area or inspection of satellite images. Overall lack of accurate information on Alaska forests hinders our ability to make accurate avalanche indication hazard maps, resulting in both overestimation and underestimation of risk in different areas. Caution is advised in interpreting this study's results in the presence of deciduous forest, especially for any PRAs below the tree line.

2.3 Downscaled Historical and Projected Climate

To estimate avalanche release depths, we obtained snow depth climatologies from the Climate Forecast System Reanalysis (CFSR) (Saha et al., 2010) for the historical period, and the National Center for Atmospheric Research Community Climate System Model, version 4 (CCSM) (Gent et al., 2011) for the future scenario, which is based on Representative Concentration Pathway (RCP) emissions scenario 8.5 (Van Vuuren et al., 2011; Meinshausen et al., 2011; Riahi et al., 2011). Lader et al. (2022) dynamically downscaled historical and projected climate states to $4\,\mathrm{km}$ resolution using the Weather Research and Forecasting (WRF) Model version 4 (Skamarock et al., 2019) and they aggregated the results to determine the maximum 3-day

https://doi.org/10.5194/egusphere-2026-1345
Preprint. Discussion started: 18 March 2026

snowfall in each year. Note that prior studies have used maximum 3-day snow accumulation (White et al., 2024), which will be a little less than maximum 3-day snowfall. Such an approach is not practical in Alaska due to uncertainties modeling snowpack accumulation.

We then took the maximum over all the years of historical period (1981–2010) and future scenario (2031–2060) to be an estimate of the maximum possible 3-day snowfall, including settling, during each of those periods. We lack long time series of reanalysis or meteorological observations for Alaska, which precludes us from developing commonly used return intervals or robust determinations of extremes (Naveau et al., 2005). The observed maximum over each scenario period may therefore underestimate the actual risk.

To achieve a higher resolution snowfall dataset that captures maritime and local topographical influences, we employed a two-step downscaling process. First, a spatially variable lapse rate, influenced by distance from the open ocean, was derived. This lapse rate was determined by analyzing snowfall differences between adjacent higher and lower elevations within the 4km dynamically downscaled historical climatology. Second, this derived lapse rate was applied in a downscaling and smoothing algorithm to produce a $10\,\mathrm{m}$ resolution 3-day maximum snowfall product, which was used to inform release depths in the PRAs. These steps are now described in greater detail:

2.3.1 Lapse Rate Computation

Following Qin et al. (2018), we computed the gradients of temperature T and elevation H by convolving each field with a 5×5 Sobel-Feldman kernels (Sobel, 2014). Using these gradients, we computed the gridded lapse rate as in Figure 4:

$$\text{Lapse Rate} = \frac{\nabla T \cdot \nabla H}{|\nabla H|^2} \tag{1}$$

where $\nabla T \cdot \nabla H$ is the component temperature change along the steepest gradient at each point.

Orographic precipitation is a major driver of snowfall in Southeast Alaska, with the total amount of snowfall diminishing with elevation *and* distance from the open ocean. The computed lapse rate (Figure 4) also varies with distance from the open ocean, providing for a different rate of change with elevation in coastal areas vs. inland. To capture this effect, we theorized a simple model in which the lapse rate depends on distance from the open ocean.

Because of the porous coastline in Southeast Alaska, computing distance to the open ocean is not straightforward. As a proxy for this number, we used the mean distance to the 30 closest ocean gridcells, producing a reasonable and smoothed field (Figure 5).

We then used a box-and-whisker plot to plot the computed lapse rate L (in mm snow per m elevation) versus computed distance from open ocean D (Figure 6). Based on this plot, we determined the following empirical rule for lapse rate L used to downscale 3-day snowfall from the historical reanalysis output of WRF:

https://doi.org/10.5194/egusphere-2026-1345
Preprint. Discussion started: 18 March 2026

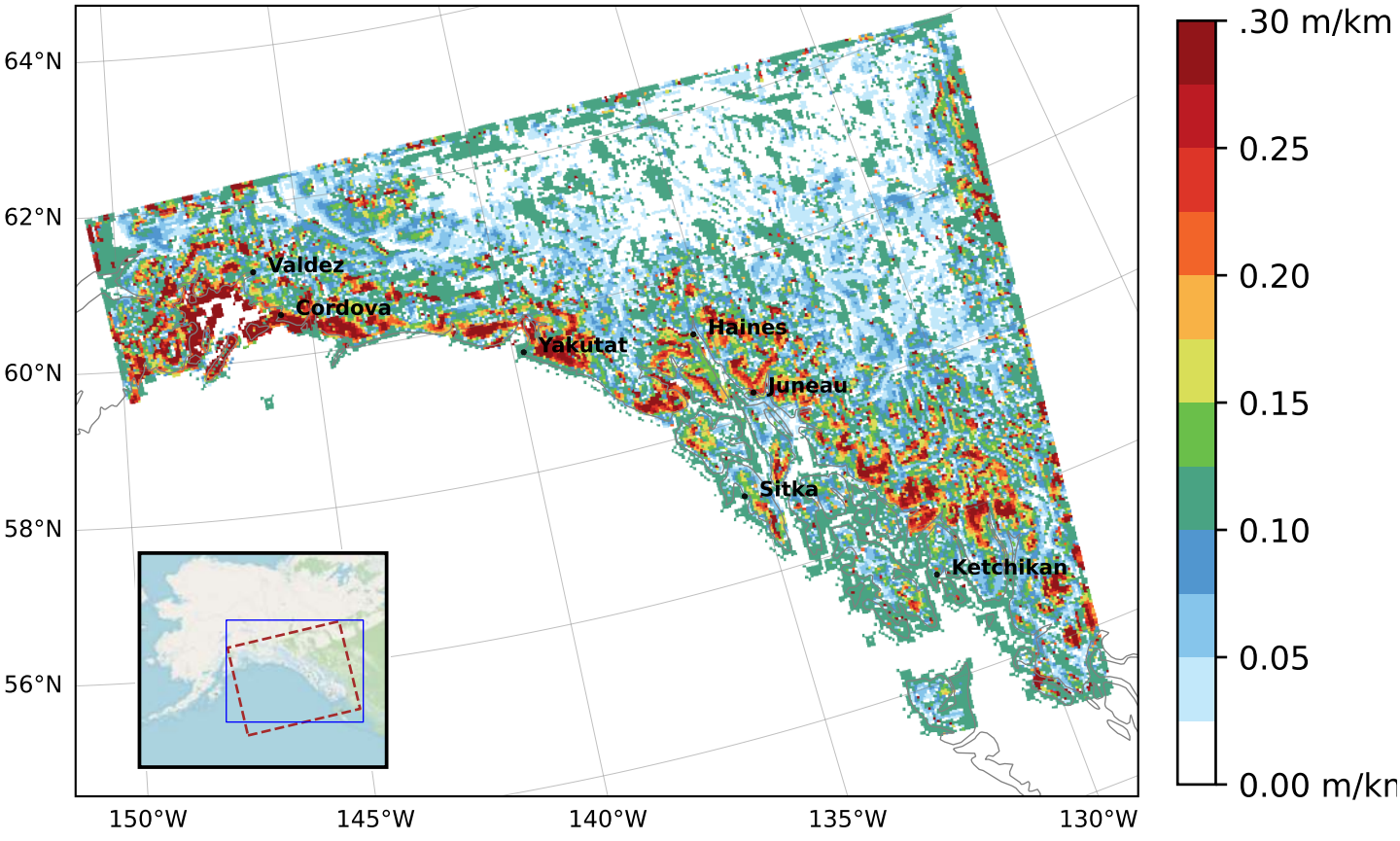

Figure 4. Lapse rate of 3-day maximum snowfall, computed by comparing adjacent $4\,\mathrm{km}$ WRF gridcells. Units are meters of snow per kilometer of elevation ($\mathrm{m/km}$), equivalent to $\mathrm{mm/m}$. **Inset Map:** The dotted red outline shows the WRF computational domain. The blue square locates the domain of the main map.

$$L = \begin{cases} 0.0923 & \text{if} \quad 0\,\mathrm{km} \le D < 90\,\mathrm{km} \\ 0.0923 + (0.373 - 0.0923)\frac{D-90}{240-90} & \text{if} \quad 90\,\mathrm{km} \le D < 240\,\mathrm{km} \\ 0.373 & \text{if} \quad D \ge 240\,\mathrm{km} \end{cases} \tag{2}$$

We apply this rule to produce a lapse rate at each WRF gridcell. In practice, a constant lapse rate of $0.0923\ \mathrm{mm}$ snow per m elevation is used because *all* of Southeast Alaska falls within $90\,\mathrm{km}$ of the coast.

2.3.2 Downscale and Smooth with Lapse Rate

Following the determination of a lapse rate for Southeast Alaska, we applied it to the $4\,\mathrm{km}$ resolution WRF maximum 3-day snowfall to generate a $10\,\mathrm{m}$ resolution dataset. This process consisted of three steps: First, we remapped the historic and projected WRF output to the $10\,\mathrm{m}$ target resolution using a nearest neighbor algorithm, resulting in a 160,000-fold increase in

https://doi.org/10.5194/egusphere-2026-1345
Preprint. Discussion started: 18 March 2026

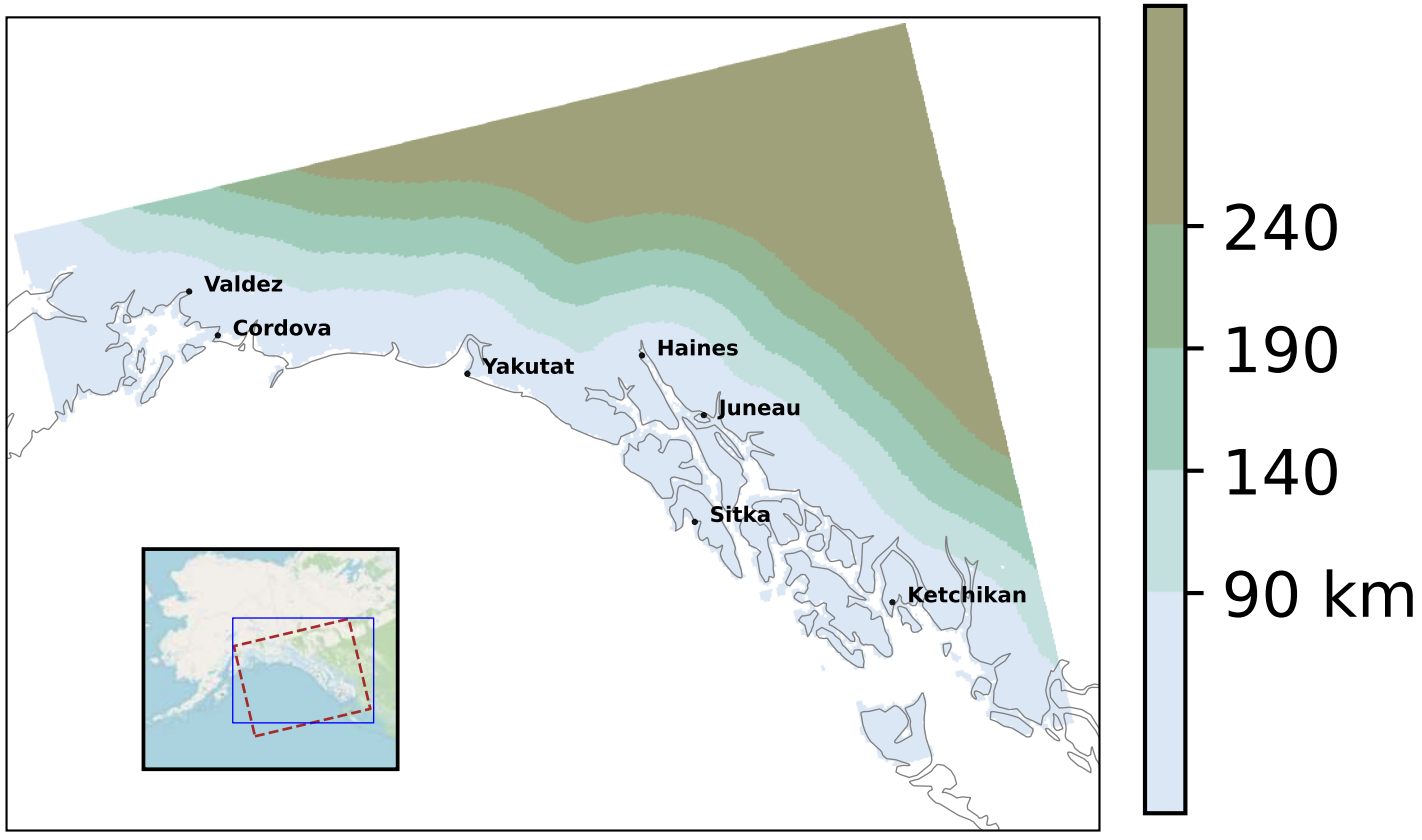

Figure 5. Distance to Open Ocean, as computed by the mean distance to the 30 closest ocean 4 km WRF gridcells. **Inset Map:** The dotted red outline shows the WRF computational domain. The blue square locates the domain of the main map.

grid cells. Second, we smoothed the resulting 10m raster by convolving it with a Gaussian kernel of width $\sigma = 4\,\mathrm{km}$ (400 grid cells). This smoothing, efficiently computed using the Fast Fourier Transform (Duhamel, 1990; Getreuer, 2013), eliminated non-physical hard boundaries between the original WRF grid cells. Finally, we applied the elevation-based lapse rate to each 10 m grid cell, adjusting the smoothed snowfall value based on the cell's elevation in the DEM.

2.4 Tiling of Alaska

Due to the large study area (Figure 1) and computational demands we devised a tiled subset approach. We created a grid of 30 km square *tiles* that cover all of Alaska, and split up the computation along tile boundaries. Tiles are labelled with an (i, j) coordinate system with $(0, 0)$ being in the far Northwest, and they are aligned to even multiples of 30 km in the EPSG:3338 coordinate system.

https://doi.org/10.5194/egusphere-2026-1345
Preprint. Discussion started: 18 March 2026

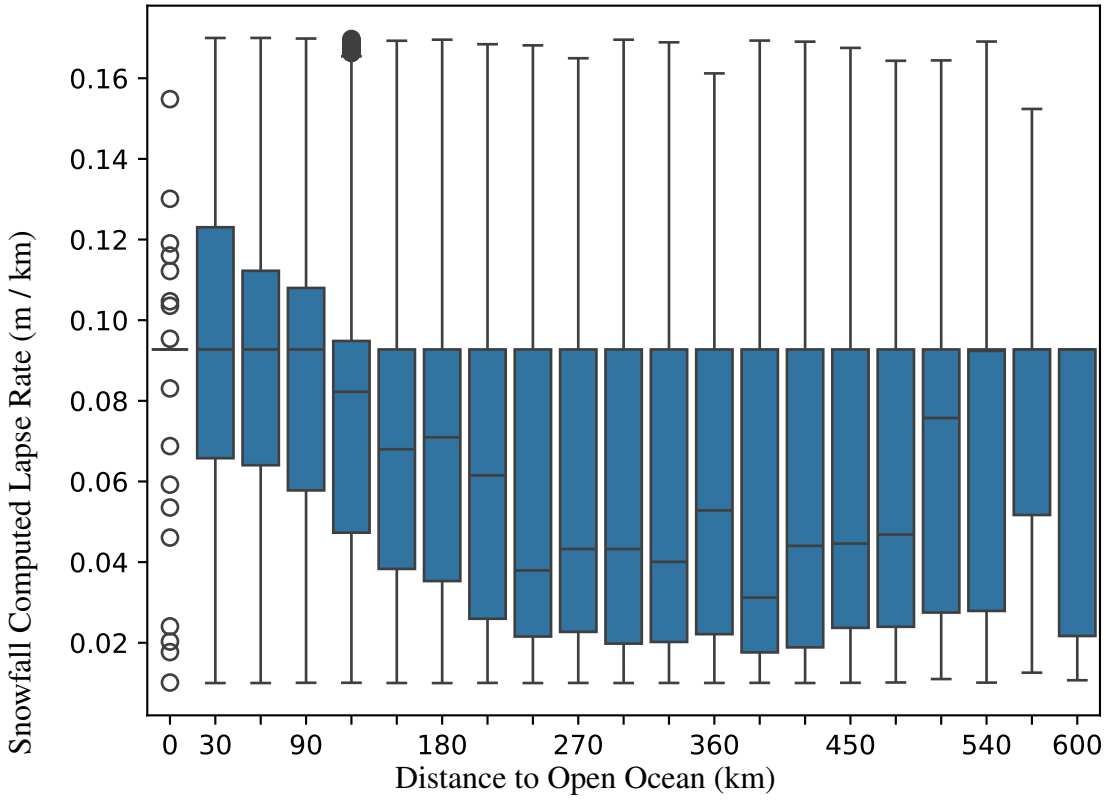

Figure 6. Distance to open ocean of 4 km WRF gridcells vs. computed lapse rate of 3-day maximum snowfall. The plot was created using the `seaborn.boxplot()` function from the Seaborn Python library. The blue box shows the quartiles of snowfall while the whiskers extend to show the rest of the distribution, sans outliers.

PRAs and avalanches only need to be computed for tiles that intersect with the WRF study area (Lader et al., 2020) and contain at least some land. We obtained this set based on a shapefile of Southeast Alaska land boundaries intersected with a shapefile for the WRF domain used for climatological reanalysis (Section 2.3).

2.5 Scenarios

For each tile we compute four scenarios: *historical-frequent*, *historical-rare*, *future-frequent*, and *future-rare*. Maximum 3-day snowfall is based on the years 1981–2010 for the *historical* scenarios and 2031–2060 for the *future* scenarios. *Frequent* scenarios generate PRAs using 30-year return periods and *rare* scenarios use a 300-year return period.

2.6 Potential Release Area (PRA) Delineation

To deliminate potential release area (PRA) polygons, we used the methods described in Buhler and Kuhne (2018) and Bühler (2018), which we summarize here. We start with the IFSAR DEM remapped to 10 m resolution and generate slope angle,

https://doi.org/10.5194/egusphere-2026-1345
Preprint. Discussion started: 18 March 2026

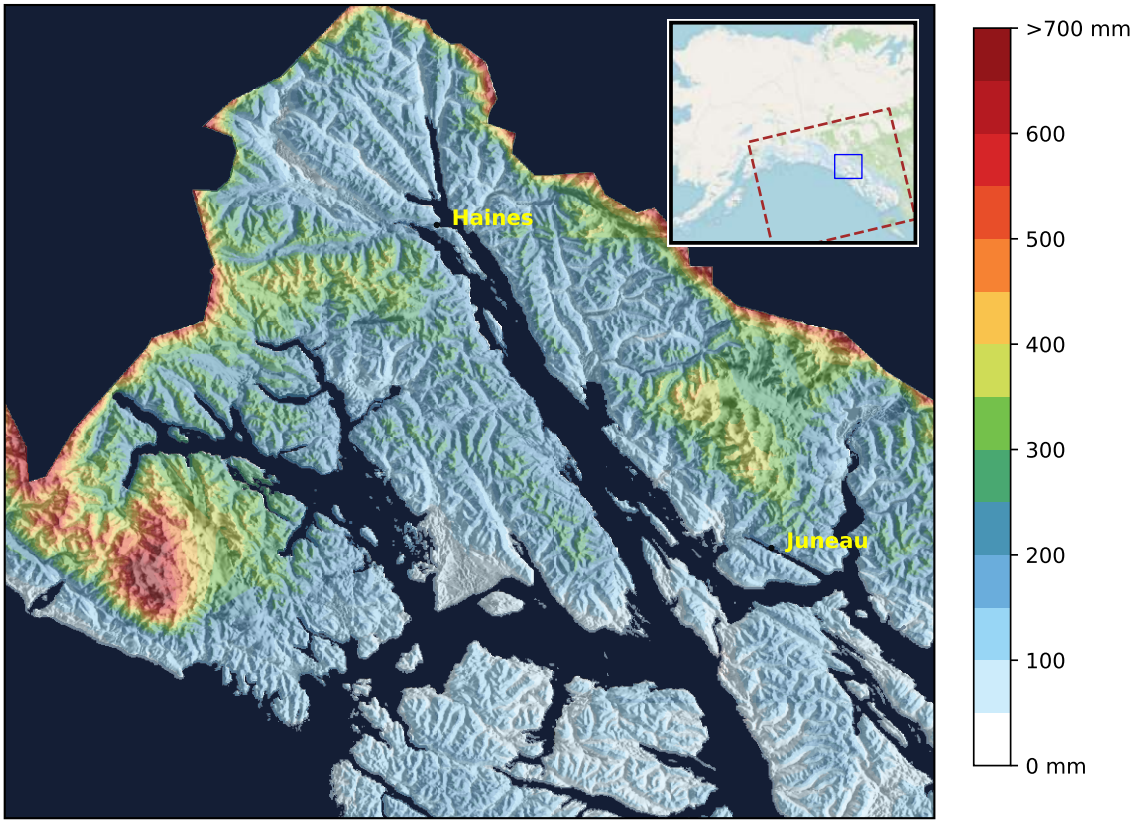

Figure 7. Three-day maximum snowfall, downscaled via lapse rate to 10 m and smoothed, for the historical period (1981-2010). **Inset Map:** The dotted red outline shows the WRF computational domain. The blue square locates the domain of the main map.

aspect sectors, plan curvature, ruggedness (Sappington et al., 2007) and fold (Schmudlach and Köhler, 2016) for the analysis. We combine these layers with the forest mask (Section 2.2) to feed an object based image analysis processing tree (Blaschke, 2010). We compute PRAs separately for the *frequent* vs. *rare* scenarios, typically resulting in larger PRAs for the rare scenario.

For a given tile, we determine PRAs in the tile (Section 2.6) and compute avalanches for those PRAs. PRAs near the edge of a tile could spawn avalanches that flow past the edge of that tile. To accommodate this, we add a margin of 7980 m to all four sides of the tile to create an expanded *compute domain* used by RAMMS::LSHIM. The margin size was chosen based on the maximum conceivable extent of an avalanche in Southeast Alaska, and also to be a multiple of 30 m, making the compute domains line up to even boundaries of the 30 m NCLD grid cells. The centroid of the convex hull is computed for each PRA, and PRAs where that centroid falls outside the tile (sans margin) are discarded.

Each PRA is categorized based on its area: *Tiny* (0–5000 m^2), *Small* (5,000–25,000 m^2), *Medium* (25,000–60,000 m^2) or *Large* (> 60,000 m^2). The size category affect basal friction and turbulent friction in RAMMS::LSHIM (Christen et al., 2010) used when simulating each avalanche (Bühler et al., 2022). Vegetation is ignored for area classes *Medium* and *Large* because destruction of the forest is assumed.

https://doi.org/10.5194/egusphere-2026-1345
Preprint. Discussion started: 18 March 2026

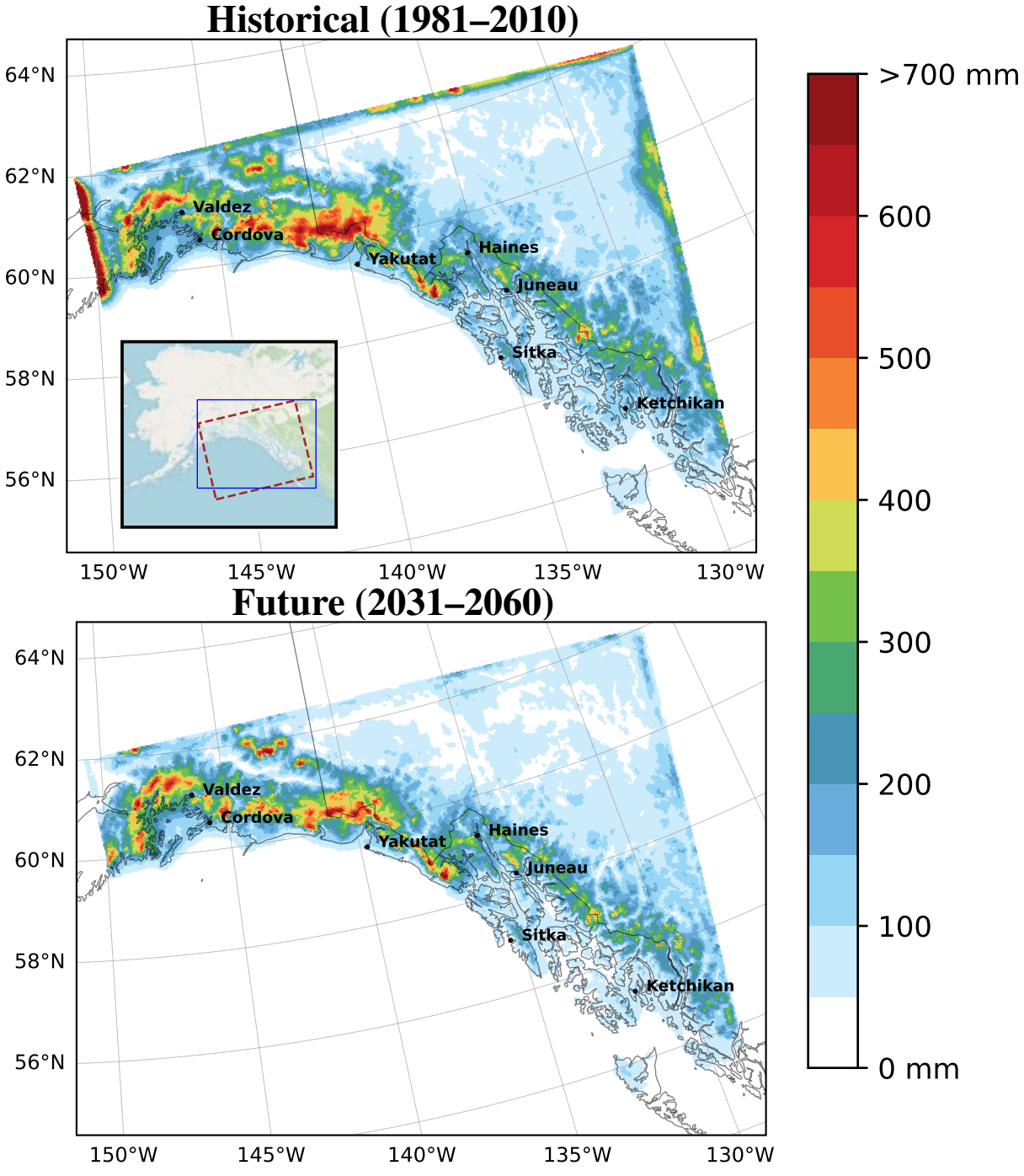

Figure 8. Historical (1981–1990) and Future (2051–2060): Maximum three-day snowfall, Southeast Alaska as computed via WRF dynamical downscaling. Edge effects produce unreliable values near the western, northern and eastern boundaries of the WRF domain. **Inset Map:** The dotted red outline shows the WRF computational domain. The blue square locates the domain of the main map.

https://doi.org/10.5194/egusphere-2026-1345
Preprint. Discussion started: 18 March 2026

This approach to categorizing avalanches based on the size of their release area is similar to previous studies. Bühler et al. (2022) classify based on snow volume rather than area in the PRA, which is equivalent to the case with a snow depth of $1\,\mathrm{m}$. Classifications are similar because maximum 3-day snow depths around Juneau are typically between $0.7\,\mathrm{m}^2$ and $1.2\,\mathrm{m}^2$. TetraTech (2022) (Appendix D) uses three size categories in which *Small* PRAs range between 391–$11,623\ \mathrm{m}^2$ with a $1\,\mathrm{m}$ release depth; *Medium* PRAs range between $3,634$–$39,422\ \mathrm{m}^2$ with a $1.5\,\mathrm{m}$ release depth; and *Large* PRAs range between $19,257$–$149,622\ \mathrm{m}^2$ with a $2\,\mathrm{m}$ release depth.

2.6.1 Repeated PRAs

The PRAs computed by the image processing tree may vary in minor ways depending on exogenous factors such as the size or extent of the compute domain in which the PRA was delineated. When a PRA straddles a tile boundary, it will be delineated in the compute domain for both tiles, resulting in two versions of the PRA. As long as the centroid of the convex hull for both versions is located in the same tile, one version will be included and the other discarded. In some cases, the two PRA versions will be assigned to the adjacent tiles based on their centroids, resulting in that PRA being repeated (see Figure 9). Repeated PRAs could be identified and removed when producing hazard indication maps; however, since such maps plot *maximum* values, such effort would make little or no difference.

2.7 Domain Builder

Once a PRA is identified, the avalanche initiating from it is simulated using the RAMMS::LSHIM finite difference code. To save memory and time, RAMMS::LSHIM is not run on the full compute domain, rather on a smaller rectangular *RAMMS::LSHIM domain* created separately for each avalanche. The RAMMS::LSHIM domain, sized based on an estimate of the expected avalanche runout, is computed in the following steps:

1. The DEM is processed to ensure continuous drainage by filling depressions and artificial sinks caused by noise or minor terrain features, using the algorithm of Zhu et al. (2013).
2. Based on the basin-filled DEM, the continuous set of gridcells with elevation equal to or lower than those of gridcells in the PRA is computed. This is, to first approximation, the set of gridcells expected to be covered by an avalanche.
3. The *minimum area bounding rectangle* (MBR) is computed for each set of gridcells using the algorithm of Freeman and Shapira (1975).
4. A margin of $1000\,\mathrm{m}$ is added to all sides of the MBR.
5. Gridcells enclosed by or intersecting with the MBR and margin are included in the RAMMS::LSHIM domain.

In some cases, the domain created in this manner, based on an initial estimate of the runout, is not large enough and the avalanche will overrun the domain. The RAMMS::LSHIM simulation is then scrapped and re-done on a larger domain, with an additional margin of $5\,\mathrm{km}$ added to all four sides. Approximately 95% of avalanche simulations complete without overruns on their initial domain, and 100% of the remaining completed on the expanded domain.

https://doi.org/10.5194/egusphere-2026-1345
Preprint. Discussion started: 18 March 2026

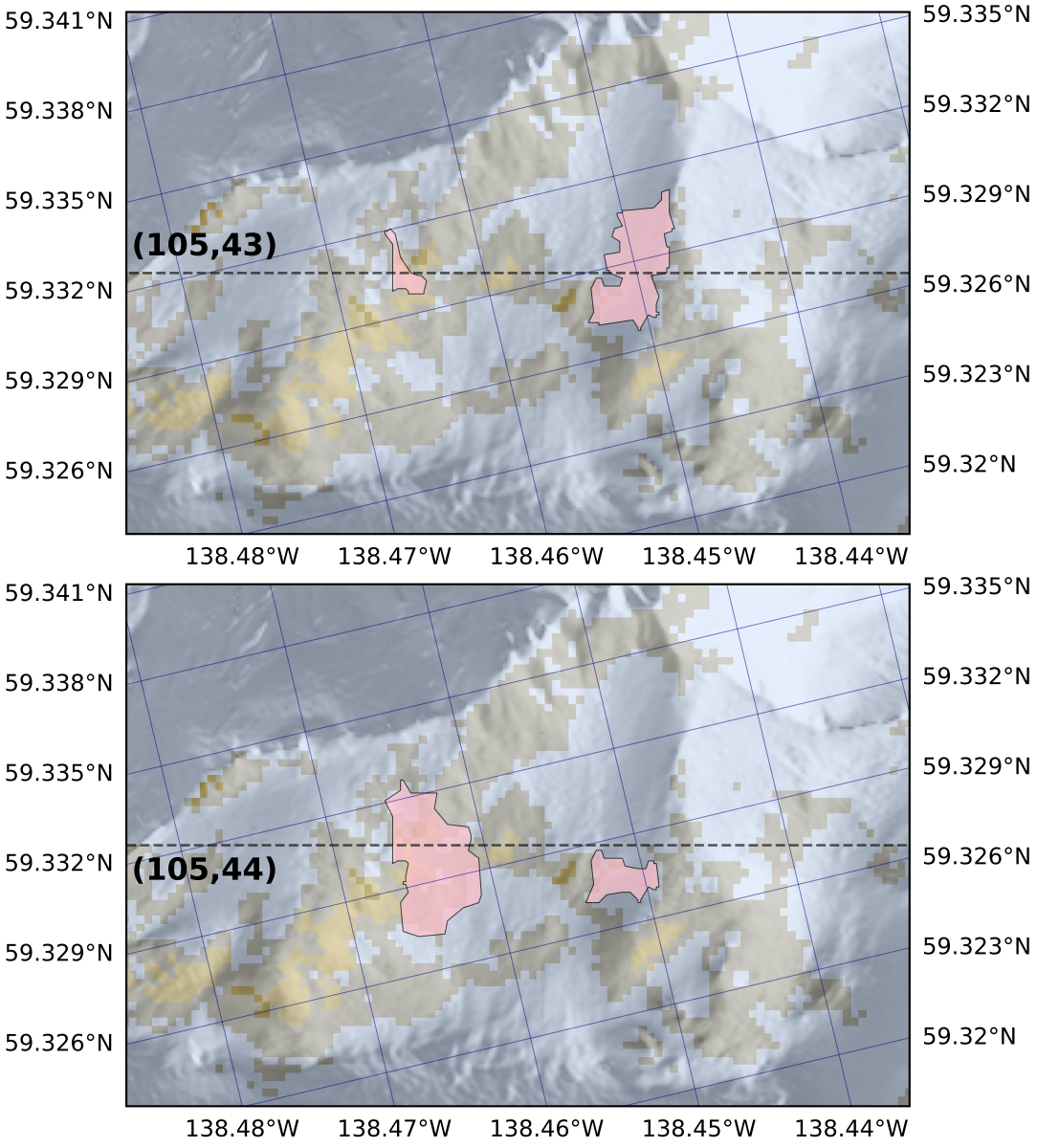

Figure 9. Very different PRA delineations for PRAs straddling the boundary between tiles shown by the dotted line. PRA generation can vary between tiles, with differing sets of PRAs generated in tile margin overlap areas. The PRAs in the top panel were computed along with others in tile $(105, 43)$ and were assigned to $(105, 43)$ based on the centroids of their convex hulls (PRAs not assigned to $(105, 43)$ were discarded). The PRAs in the bottom panel were computed along with others in the tile $(105, 44)$. They were different enough from their corresponding PRAs in the top panel to be assigned to $(105, 44)$ based on the centroid of *their* convex hulls. Thus these PRAs are represented twice.

https://doi.org/10.5194/egusphere-2026-1345
Preprint. Discussion started: 18 March 2026

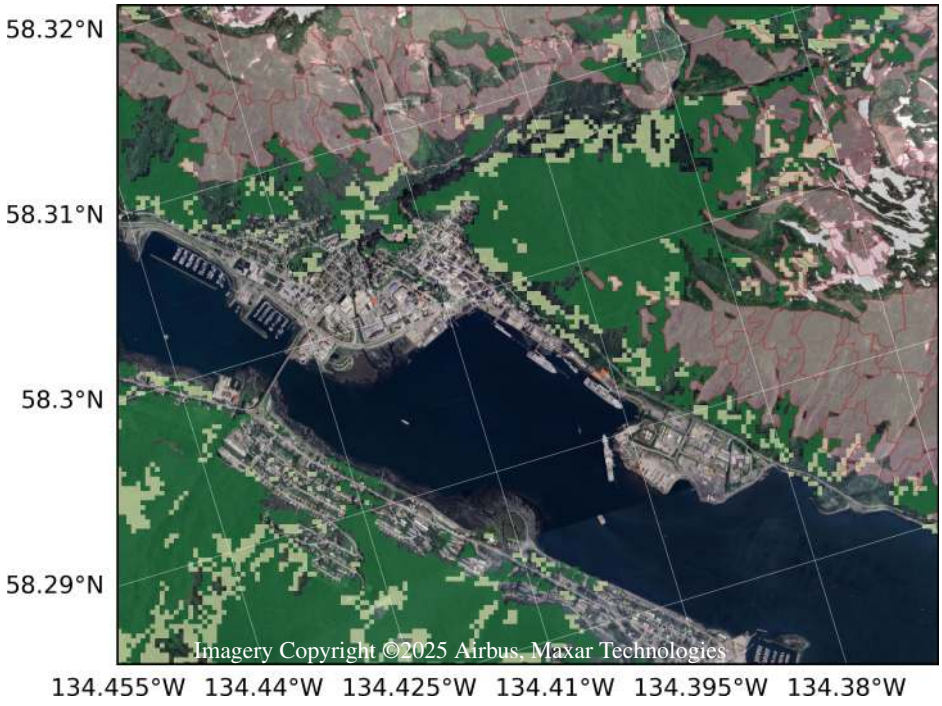

Figure 10. Potential Release Areas near Juneau downtown for the *historical-frequent* scenario. Only PRAs for avalanches that were kept by the filter algorithm (Section 3.1.1) are shown. See Figure 12 for corresponding avalanche extents.

2.8 Release Depths

Bühler et al. (2022) use climatological snowfall observations at the centroid of each PRA to determine a release depth d_0 through a series of corrections for elevation, drifting snow and the slope gradient. None of these corrections, specific for the Alps, are possible for most of Alaska given the sparsity of observations. Therefore we use the downscaled climatological snowfall d (Section 2.3) to calculate the snow depth, d_0, perpendicular to the slope angle θ: $d_0 = d\cos(\theta)$.

2.9 Numerical Avalanche Modeling with RAMMS::LSHIM

Following the methods of Bühler et al. (2022), RAMMS::LSHIM is run separately for each PRA and compute domain delineated above for each of the four scenarios. The RAMMS::LSHIM parameters are set based upon the standard approach for avalanche hazard mapping in Switzerland. Curvature effects for the friction are considered (Fischer et al., 2012), the cohesion is set to $50\,\mathrm{Pa}$, and the stop criterion is set to 5% of the total momentum. Based on these input datasets, all individual PRAs were simulated with RAMMS::LSHIM (Bühler, 2018) as individual avalanches, not interacting with each other. We performed these calculations on an HTCondor Linux cluster with 184 cores.

https://doi.org/10.5194/egusphere-2026-1345
Preprint. Discussion started: 18 March 2026

2.10 Extent Outlines

After avalanches simulations were complete, we computed *extent polygons* for each avalanche, incorporating gridcells with flow depth at least $0.25\,\mathrm{m}$ and velocity at least $1\,\mathrm{m}$ (Bühler et al., 2022). Discontinuous extent polygons near the terminus are an artifact of this kind of thresholding. Alternative extent polygons were computed to correspond to the *moderate* (maximum pressure at least $1\,\mathrm{kPa}$) and *severe* (maximum pressure at least $30\,\mathrm{kPa}$), allowing more direct comparison with detailed local avalanche studies from TetraTech (2022).

2.11 Low Elevation Avalanches

Low elevation avalanches — those originating below the treeline — may occur in recently deglaciated landscapes or in areas recently disturbed by unstable slope processes, and are commonly produced by the algorithm of Bühler et al. (2022). They are rare in Cordova but common in Valdez due to steep, newly exposed fjord-valley sidewalls below the trim line that do not yet have forest cover. In Juneau, however, the algorithm produces low elevation avalanches that start in areas with a complex patchwork of forest types, much of it misclassified in the NLCD data. Due to inherent complexity and lack of data, low elevation avalanches initiating in partially forested areas are outside of the scope of this study.

To address these cases, low elevation avalanches — those initiating under $300\,\mathrm{m}$ elevation — are filtered out after they have run based on the NLCD classifications encompassed by their PRA and extent polygons. Avalanches are ruled out if either: (a) the PRA contains at least 30% Deciduous or Mixed Forest type; or (b) the extent contains at least 30% Evergreen or Mixed Forest types (See Section 3.1.1 for more).

3 Results and Discussion

Our automated hybrid modeling approach for Southeast Alaska allowed us to run over 3.5 million simulations, which were assembled into each tile they intersect to produce comprehensive avalanche hazard indication maps for both recent historic and future climates (Figure 11). The tiles were assembled using ArcGIS into a single high-resolution interactive map for the study region, offering stakeholders an easily browsable tool for evaluating susceptible terrain. Specifically, the map visualizes avalanche extent and three key variables, maximum pressure, maximum velocity, and maximum flow depth, for frequent and rare scenarios across represented climatologies (Section 3).

3.1 Validation

Validating these maps is a critical challenge due to the sparse knowledge of avalanche hazards in Alaska, which is largely confined to experiential and anecdotal observations in settled areas. However, we were able to validate and refine our approach by comparing our results to the more comprehensive, localized hazard studies available for Valdez (Fesler and Fredson, 2000) and Juneau (WSL Institute, 2011; TetraTech, 2022), as detailed in this section. These are the only publicly available studies in Southeast Alaska, and validating against them increases confidence in our results across the entire region. Outside of these

https://doi.org/10.5194/egusphere-2026-1345
Preprint. Discussion started: 18 March 2026

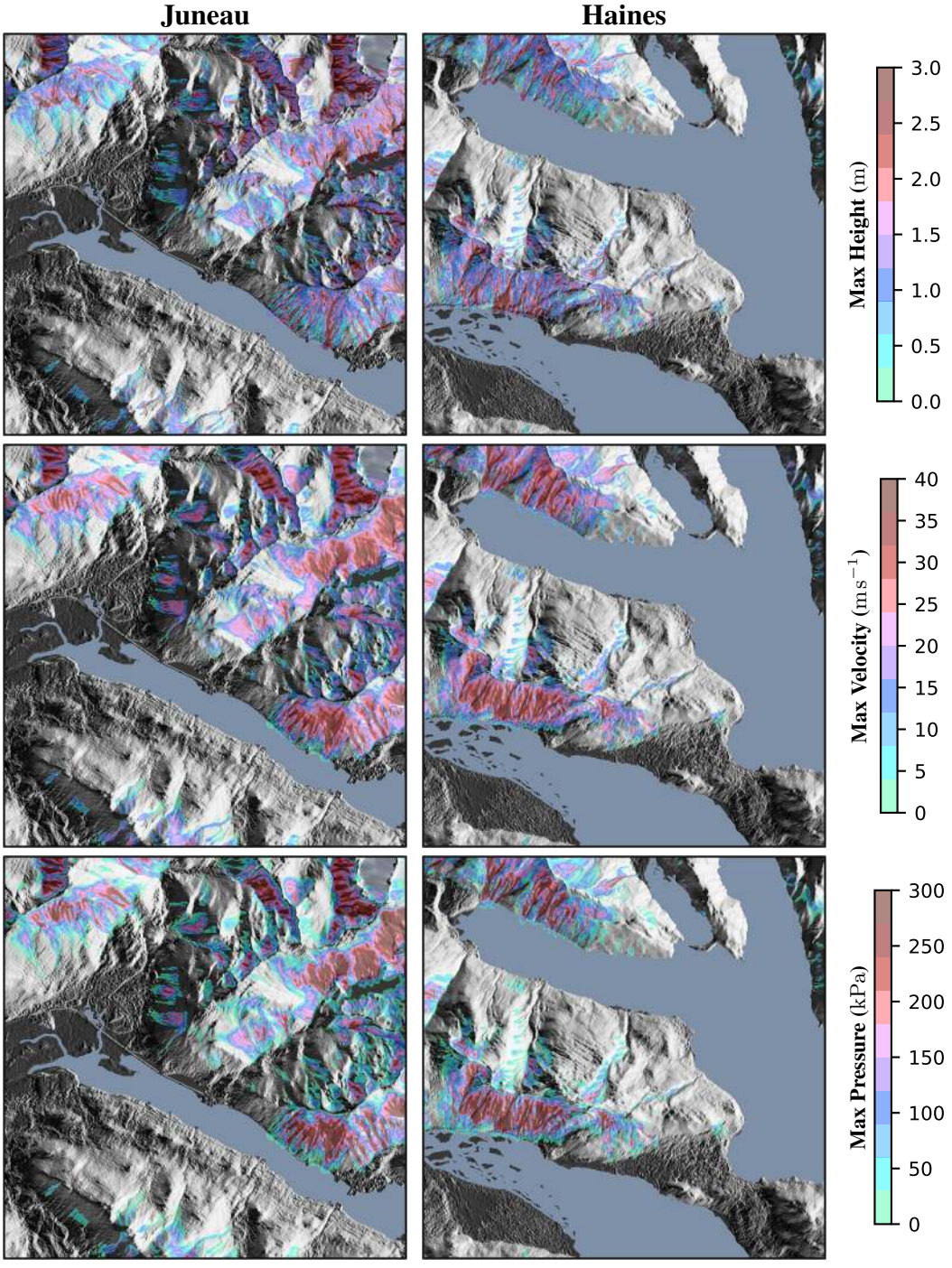

Figure 11. Maximum height, maximum pressure and maximum depth hazards for Juneau and Haines regions. Results compute for the *historical-frequent* scenario.

https://doi.org/10.5194/egusphere-2026-1345
Preprint. Discussion started: 18 March 2026

settled areas, our browsable map serves as the first and best systematic hazard indication and awaits further validation against future observations and more sophisticated modeling efforts.

3.1.1 Juneau Validation

WSL Institute (2011) used RAMMS::LSHIM to study the Behrends Ave and White Subdivision avalanche paths on Mt. Juneau, both of which have caused significant property damage in the past. More recently, TetraTech (2022) integrated the best available resources in a single high quality study. The study used three debris flow models, including RAMMS::LSHIM. RAMMS::LSHIM defaults based on European data were adjusted based on "field evidence, historical imagery review, historical avalanche occurences, local snow climate, and previous reports" in consultation with nine local avalanche experts. They analyzed 9 large-scale avalanche paths, 12 medium-scale paths and 31 small-scale paths in a high-risk study area around developed sections of Juneau measuring $7.4\,\mathrm{km} \times 2.5\,\mathrm{km}$. The result is the best possible study for this area at this time, which we compare with our hazard indication maps for validation.

In undisturbed areas of Southeast Alaska, continuous forest cover extends from the shoreline up to the treeline. This inhibits low-elevation avalanches, defined by those originating below the treeline, and hazards are largely confined to large high-elevation avalanches that are able to clear forest corridors and extend their runout down to the ocean. For this reason, TetraTech (2022) focused on high-elevation avalanches, which present a clear and present danger.

Our study takes a different approach, including low-elevation PRAs, and then filtering them out post-hoc if they were implausible (Section 2.11). The situation in Juneau is complicated because vegetation on the city's low elevations has been disturbed multiple times by human and natural forces, leaving a diverse and complex set of vegetation that shows up in the NCLD data as a checkerboard of forest cover types. Our filter algorithm performed well in spite of this uncertainty and complexity, successfully filtering out implausible avalanches but leaving known hazards at low elevations.

The Juneau Rock Dump industrial area, built on mine tailings, sits in a hazardous area beneath a slope of Mt. Roberts that largely lacks forest. TetraTech (2022) focused on high elevation avalanches and estimated runouts and hazards for portions of the Rock Dump closest to the mountain (Figure 13). This largely matches with our analysis of high elevation avalanches. However, our study also found that avalanches could initiate in lower elevation treeless areas not considered by TetraTech (2022), thereby adding to the overall understanding of avalanche hazards.

Behrends Avenue, northwest of downtown Juneau, is situated underneath a large treeless avalanche path that has been known to present serious hazards since 1949 or before (Dickson, 2021). In spite of the possible risks, Behrends Avenue was developed with residential houses in the 1950's, buildings that remain today. A destructive avalanche in 1962 catalyzed further studies, which have increased in technical sophistication over the years and only served to reinforce the hazardous nature of the area (Mears et al., 1992; WSL Institute, 2011). Compared to our study, WSL Institute (2011) was more optimistic regarding the ability for the forests to funnel avalanche flow and protect homes below from catastrophic damage (Figure 14). This discrepancy underscores the need for further understanding of forests and their role in avalanches in Southeast Alaska.

https://doi.org/10.5194/egusphere-2026-1345
Preprint. Discussion started: 18 March 2026

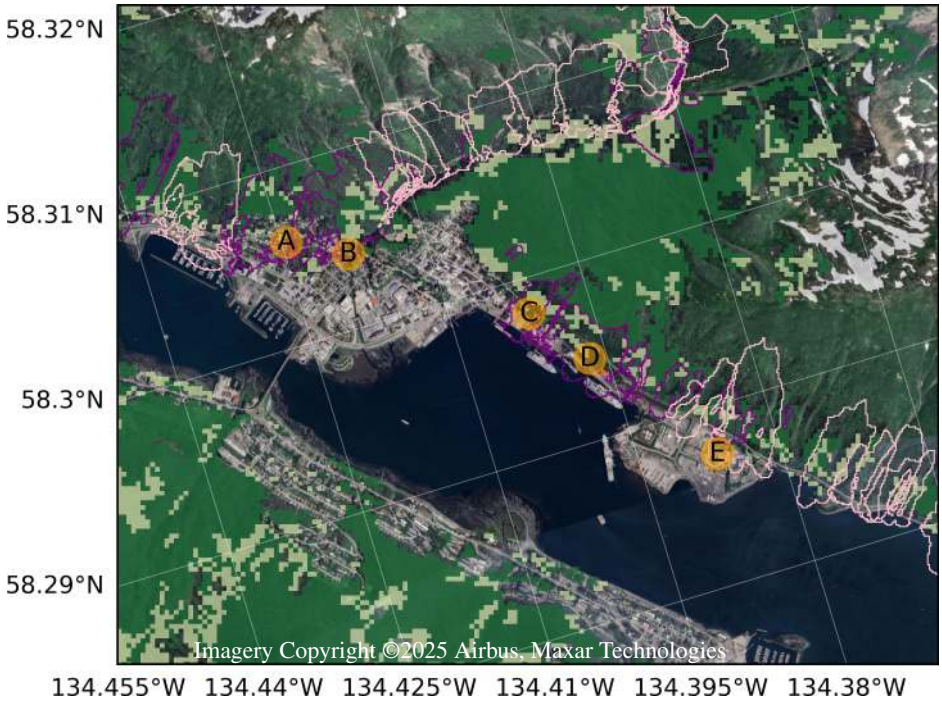

Figure 12. Extents of low elevation simulated avalanches near downtown Juneau. Purple avalanches were ruled out by the filter algorithm, and pink avalanches were kept. The results comport with local knowledge. Points A, B, C and D are known to not be subject to avalanche hazard, they have been built up, and nearby avalanches are filtered out due to the extensive Evergreen and Mixed Deciduous land surface types they encompass. Point E is subject to an avalanche on the lower reaches of a barren slope, it is known to be hazardous, and is kept by the algorithm

Further south on Thane Red is *Snowslide Creek*, a well known and largely treeless avalanche path. Our simulations finds several PRAs, both high and low elevation, that funnel some or all of their of their snow into Snowslide Creek (Figure 15). This is the expected result based on the known hazards.

3.1.2 Valdez Validation

Valdez sits at the base of mostly treeless slopes, a result of a long history of resource exploitation (Wooley, 2002), with heavy snowfall and thus frequent avalanches inhibiting regrowth. Valdez High School lies at the foot of Town Mountain with south-facing slopes that receive increased insolation capable of destabilizing snowpack. The school's gymnasium has been hit by avalanches at least twice between 1978 and 2000. Its parking lot is known to be at even greater risk, and houses on nearby Porcupine St. having been hit "a few times" in the same period. This prompted an expert assessment (Fesler and Fredson, 2000), which confirmed the risks to the high school, parking lot and nearby Porcupine St.

Our filter algorithm includes most low elevation avalanches in Valdez (less than $300\,\mathrm{m}$), accurately reflecting real risk in a deforested area. Most of these low elevation avalanches do not add to the already-present risk from high elevation avalanches.

https://doi.org/10.5194/egusphere-2026-1345
Preprint. Discussion started: 18 March 2026

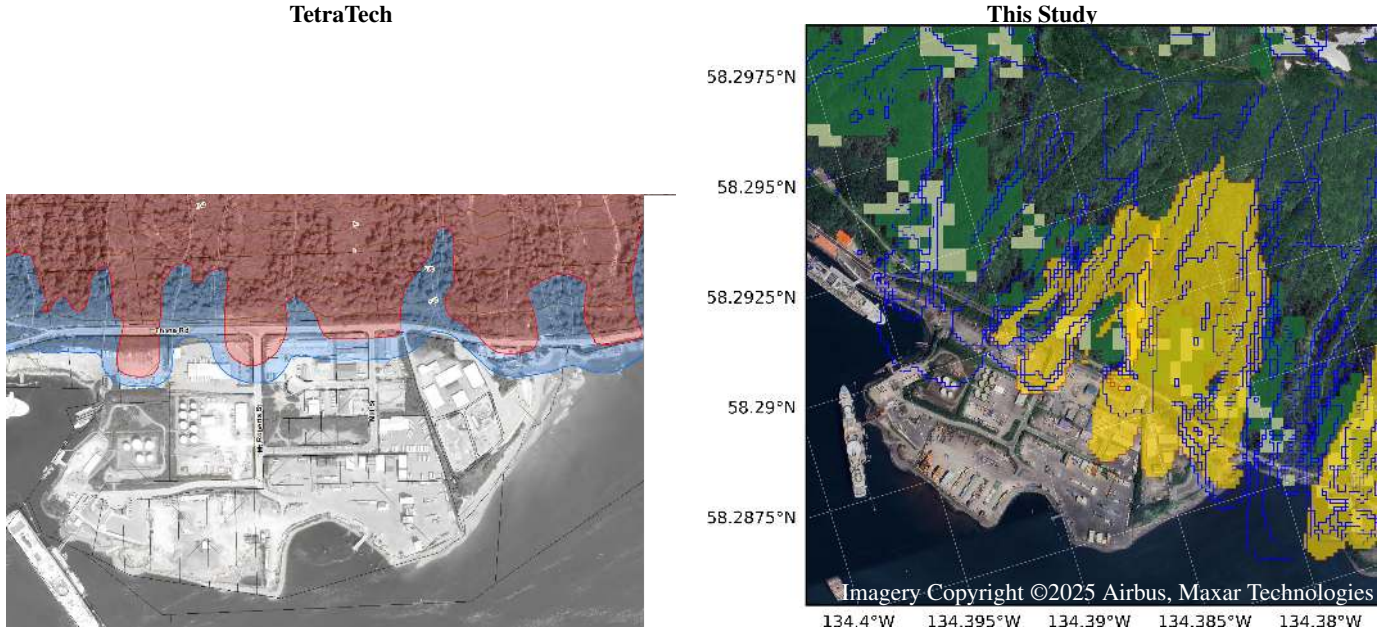

Figure 13. Avalanche hazard assessments for the Juneau Rock Dump area, which is built on mine tailings placed in the Gastineau channel. **Left**: Expert assessment (TetraTech, 2022), Copyright 2022 by TetraTech. Blue areas indicate moderate risk: return period between 30 and 300 years and impact pressure less than 30 kPa. Red areas indicate severe risk: return period less than 30 years, and/or impact pressure $\geq$ 30 kPa. **Right**: Avalanche hazards simulated in this study, *historical-frequent*, with extents cut off at at flow depth < 0.25 m or velocity $\leq 1\,\mathrm{m\,s^{-1}}$. Yellow avalanche extents originated from low elevation PRAs (less than 300 m), whereas blue outlines originated from high elevations (greater than 300 m). Areas covered in Evergreen Forest (dark green) or Deciduous Forest (light greet) are overlaid on top of the satellite view of the area. Differences between the two studies are partially attributed to lack of low elevation avalanches in TetraTech (2022).

Valdez High School is an exception because the slopes behind it are less than 300 m tall. Our filter algorithm correctly identifies these avalanche hazards, although with somewhat greater runout than Fesler and Fredson (2000) (Figure 16).

3.1.3 Cordova Validation

In contrast to Valdez, Cordova's lower elevation slopes are heavily forested with evergreen trees. This is effective at preventing low elevation avalanches, in fact, the filter algorithm filters almost all of them out. High elevation avalanches are still prevalent due to lack of tree cover above the natural tree line; however, the mountains directly beside Cordova are low elevation only. Hence Cordova in general is not exposed to significant avalanche hazard.

However, Cordova *does* illustrate some limitations in our data. Bear Country Lodge sits on the waterfront in a large high elevation avalanche runout zone, visible in satellite images of the area. Our study accurately simulates the main runout (Figure 17). However, RAMMS::LSHIM was not able to simulate smaller avalanche tracks, visible in the satellite image to the west of the main track, for a few reasons. First, the low 30 m resolution of the NLCD dataset, as compared with the 10 m resolution

https://doi.org/10.5194/egusphere-2026-1345
Preprint. Discussion started: 18 March 2026

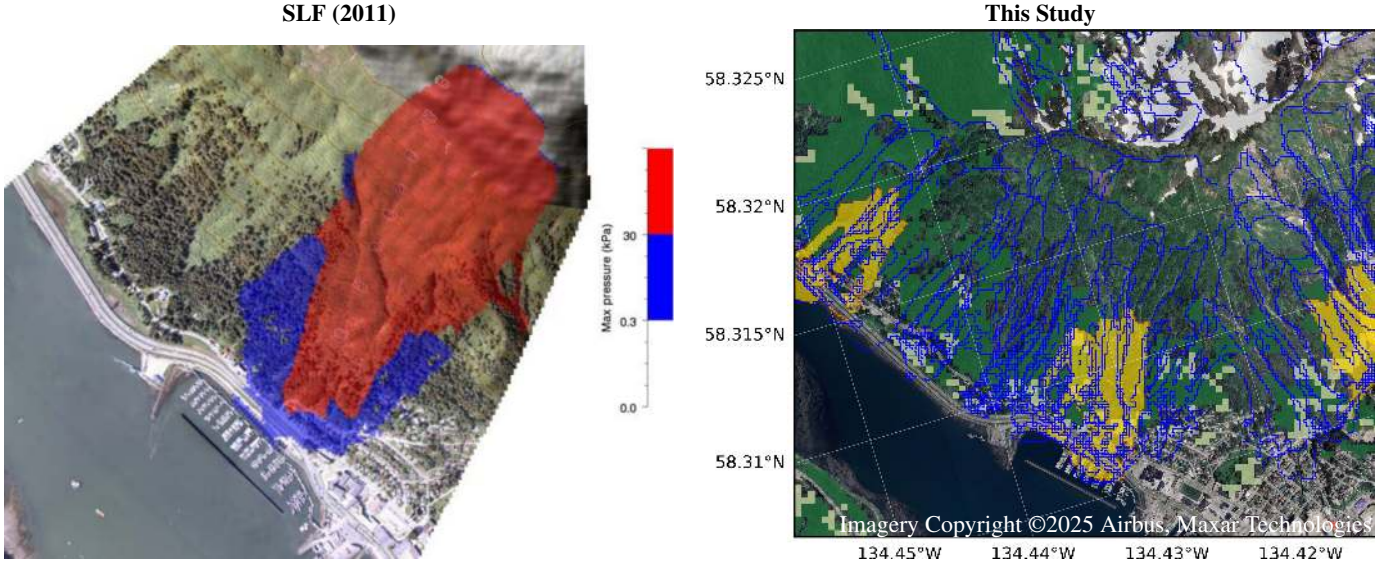

Figure 14. Avalanche hazard assessments for the Behrends Avenue area. **Left**: Expert assessment for frequent scenario (WSL Institute, 2011). Blue areas indicate impact pressure $< 30\,\mathrm{kPa}$ and blue areas indicate pressure $> 30\,\mathrm{kPa}$. **Right**: Avalanche hazards simulated in this study, *historical-frequent*, with extents cut off at at flow depth $< 0.25\,\mathrm{m}$ or velocity $\leq 1\,\mathrm{m\,s^{-1}}$. Yellow avalanche extents originated from low elevation PRAs (less than $300\,\mathrm{m}$), whereas blue outlines originated from high elevations (greater than $300\,\mathrm{m}$). Areas covered in Evergreen Forest (dark green) or Deciduous Forest (light greet) are overlaid on top of the satellite view of the area.

used with RAMMS::LSHIM, limits the ability of RAMMS::LSHIM to resolve narrow avalanche tracks. Furthermore, Figure 17 shows NLCD mis-classified areas as *Evergreen Forest* even when the satellite images clearly show this is not the case. Mis-classification of forest presence or types is a persistent problem in the NLCD data, and the results from RAMMS::LSHIM must be interpreted subject to this limitation.

3.2 Future vs. Historical Scenarios

Due to the scarcity of flat, low-elevation terrain in Southeast Alaska, we categorized development potential based on existing infrastructure patterns. We define two primary land-use categories: the 'buildable zone' as land below $40\,\mathrm{m}$, where the vast majority of Juneau's structures are located, and the 'marginal zone' as terrain between $40\,\mathrm{m}$ and $160\,\mathrm{m}$, where the rest of Juneau's buildings are located. Out of $165{,}440\,\mathrm{km}^2$ of land in our Southeast Alaska domain, only $13{,}664\,\mathrm{km}^2$ (8.3%) and $19{,}704\,\mathrm{km}^2$ (11.9%) is in the buildable and marginal zones, respectively.

To quantify avalanche risk in critical infrastructure areas, we computed hazard statistics for both buildable and marginal zones across contemporary and future climate scenarios. Using the historical frequent case as a baseline, we found that 4.5% of the buildable zone and 12.2% of the marginal zone are currently susceptible to avalanche hazards (Figure 18'). Although Southeast Alaska is projected to become warmer and wetter (Lader et al., 2022; Littell et al., 2018), the area at risk to avalanche hazard under the frequent-case scenario is expected to decrease to 3.8% ($95\,\mathrm{km}^2$) in the buildable zone and 11.0% ($236\,\mathrm{km}^2$)

https://doi.org/10.5194/egusphere-2026-1345
Preprint. Discussion started: 18 March 2026

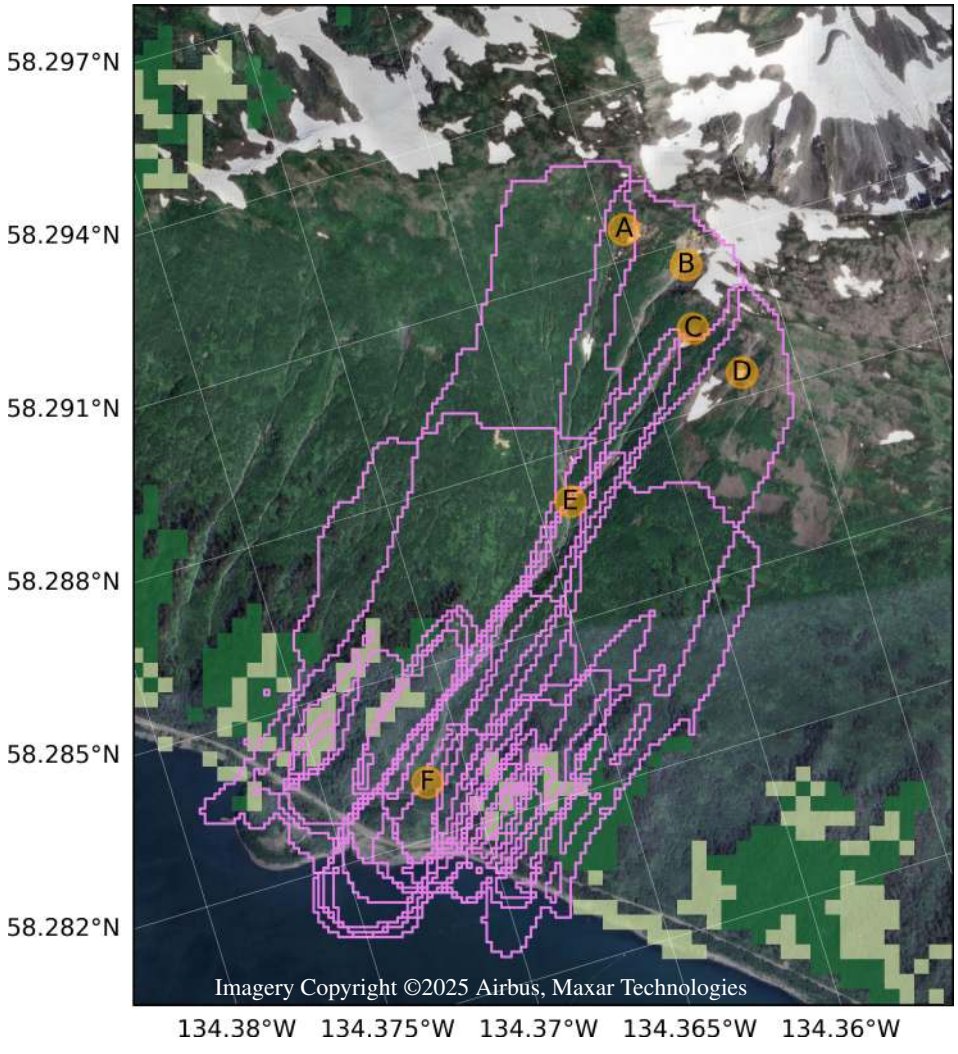

Figure 15. *Snowslide Creek* is a well known and treeless avalanche path southeast of the Juneau Rock Dump, visible in this satellite image by its deep gullies. Areas covered in Evergreen Forest (dark green) or Deciduous Forest (light greet) are overlaid on top of the satellite view of the area. Gullies begin at points A, B, C and D, then merge into a single avalanche track at E, and then fan out into a delta at F. The extent of all avalanches reaching point F are shown as violet outlines. Areas adjacent to F are subject to hazard from these avalanches because some avalanches split into multiple channels as they hit the tree line.

https://doi.org/10.5194/egusphere-2026-1345
Preprint. Discussion started: 18 March 2026

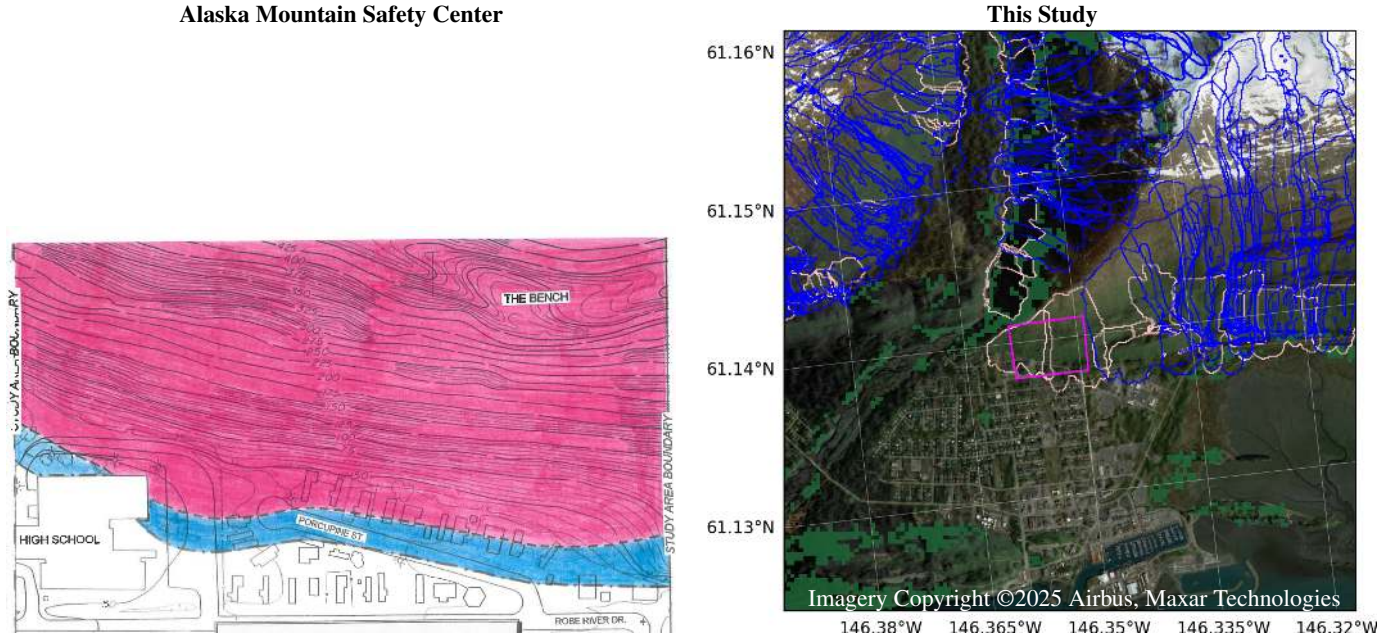

Figure 16. Avalanche hazard assessments for Valdez High School, whose gymnasium has been hit by multiple avalanches in the recent past. **Left**: Expert assessment (Fesler and Fredson, 2000). Blue areas indicate moderate risk: return period between 30 and 300 years and impact pressure less than 30 kPa. Red areas indicate severe risk: return period less than 30 years, and/or impact pressure $\geq 30\,\mathrm{kPa}$. **Right**: Avalanche hazards simulated in this study, with extents cut off at at flow depth $< 0.25\,\mathrm{m}$ or velocity $\leq 1\,\mathrm{m\,s^{-1}}$. Pink avalanche extents originated from low elevation PRAs (less than 300 m), whereas blue outlines originated from high elevations (greater than 300 m). Areas covered in Evergreen Forest (dark green) or Deciduous Forest (light green) are overlaid on top of the satellite view of the area. The fuchsia inset rectangle shows the approximate location of the map on the left.

in the marginal zone. Similar reductions were observed for rare-event scenarios. Note that these results represent a single emissions pathway (RCP8.5), and uncertainty across scenarios has not been explored.

These trends are not spatially uniform due to regional variations in projected snowfall. We expect lower elevations will experience more rain and less snow, hence a decline in maximum 3-day snowfall in most parts of the region. However, high elevations in areas of northern Southeast Alaska create conditions where the increased winter precipitation more than offsets the shift to rain, and therefore maximum 3-day snowfall increases (Figure 19a). These precipitation changes are the main driver of changes in avalanche risk (Figure 19b), and overall avalanche risk is expected to decrease. Note that this study does not address non-avalanche hazards and we cannot draw conclusions on changes in the overall combined risk for the *future* scenario.

The above numbers are averages; we can see how individual towns are expected to be affected under the *future* scenario by analyzing statistics on a $100\,\mathrm{m} \times 100\,\mathrm{m}$ grid (Figure 20). The regional differences observed in Figure 19b now become apparent

https://doi.org/10.5194/egusphere-2026-1345
Preprint. Discussion started: 18 March 2026

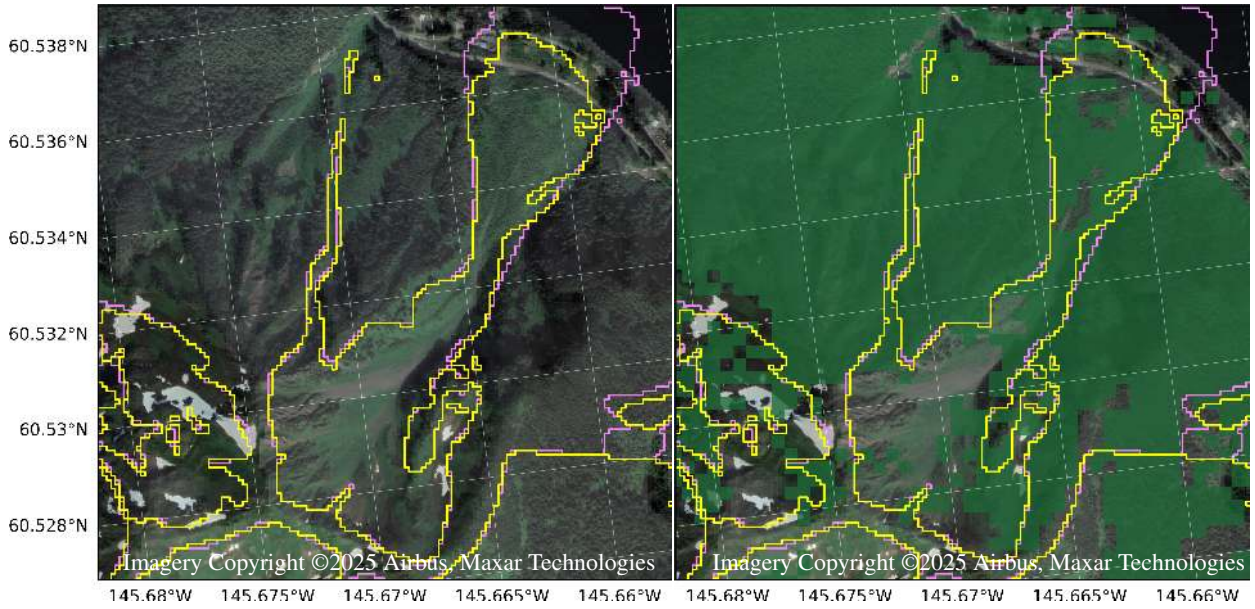

Figure 17. RAMMS::LSHIM simulation avalanche outlines above Bear Country Lodge in Cordova: yellow outlines are for 30 year return intervals, and violet outlines are for 300 year. The left plot shows narrow avalanche tracks to the west of the large avalanche, visible in the satellite image. The right plot shows the same, with 30 m forest cover plotted on top, based on the *Evergreen Forest* (42) classification of the 30 m resolution NLCD landcover data.

at a granular level, allowing estimaation of the approximate amount potential extent runouts are expected to retreat in Juneau, but advance in Haines. The on-line map may be used to further browse these results.

3.3 Regional Implementation and Modeling Constraints

Avalanche hazard mapping in Alaska is limited to select areas, primarily those with existing infrastructure, due to the high cost of collecting necessary in situ meteorological and avalanche data across the state's vast, less-populated regions. While avalanche risk has been qualitatively recognized in Alaska for decades (Hackett and Santeford, 1980), our study is the first to systematically produce hazard indication maps for Southeast Alaska, a region where this specific hazard was previously undocumented. Numerous future applications are expected for these new maps, for example planning and siting of infrastructure and development in Southeast Alaska, and risk assessment.

Evaluations against past studies reveal general agreement but highlight differences in the lower hazard boundaries of individual paths. A primary driver of these discrepancies is our modeling methodology, which uses objective PRA mapping and downscaled snow climatology data to force simulations. This shift, along with our focus on the return periods of release areas rather than impact zones, results in a more conservative hazard footprint. Given the absence of historical incidence data (Peitzsch et al., 2023), this approach ensures maximum safety, though it necessitates further analysis of its practical alignment with traditional expert mapping.

https://doi.org/10.5194/egusphere-2026-1345
Preprint. Discussion started: 18 March 2026

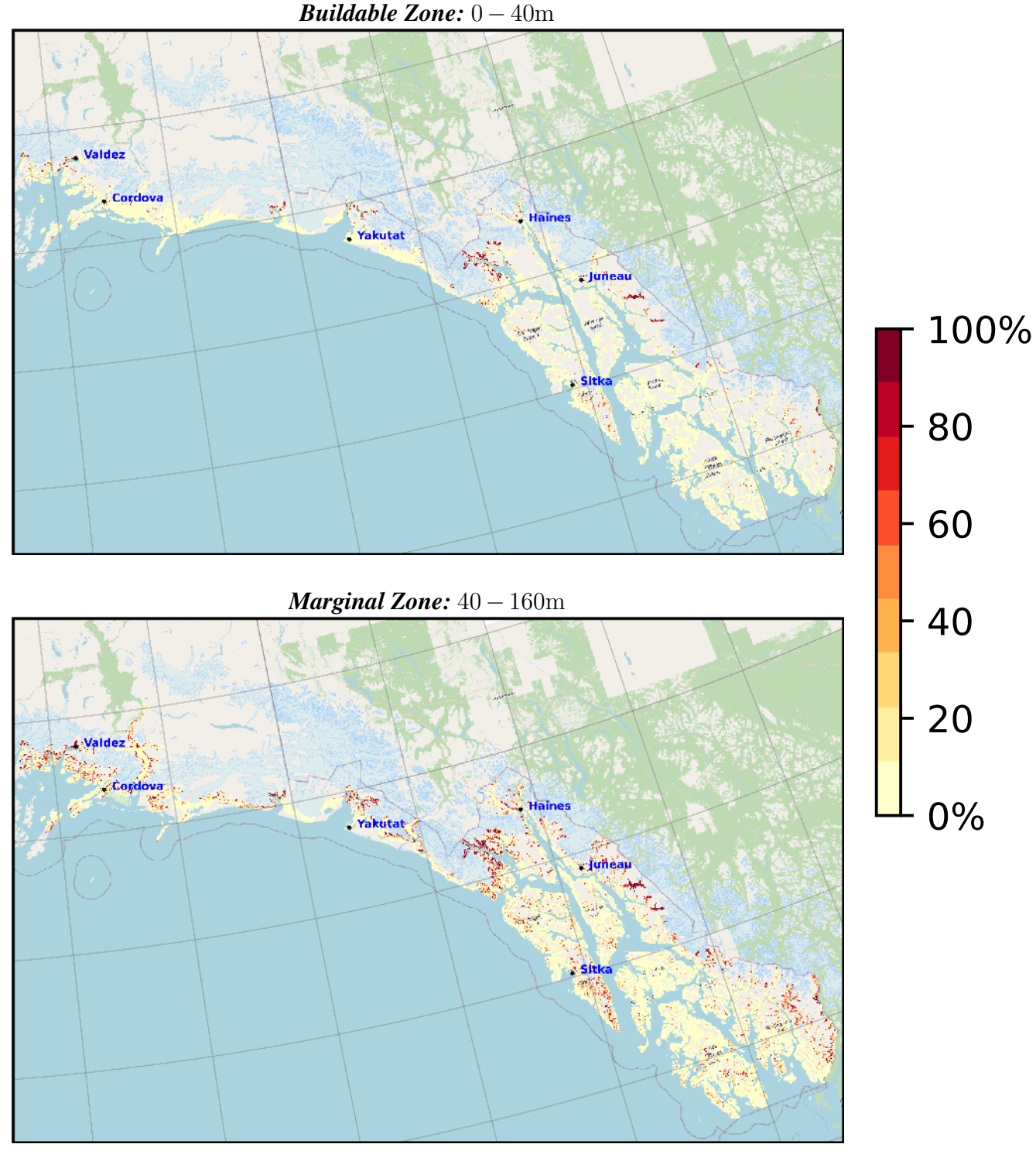

Figure 18. Baseline avalanche risk by elevation. Plot shows the portion of land within the *buildable* and *marginal* elevation zones at risk under the *frequent-historical* scenario. In most but not all areas, the most valuable land for development — that below 40 m elevation — is also least subject to avalanche risk. Not surprisingly, higher elevation areas carry increased avalanche risk.

https://doi.org/10.5194/egusphere-2026-1345
Preprint. Discussion started: 18 March 2026

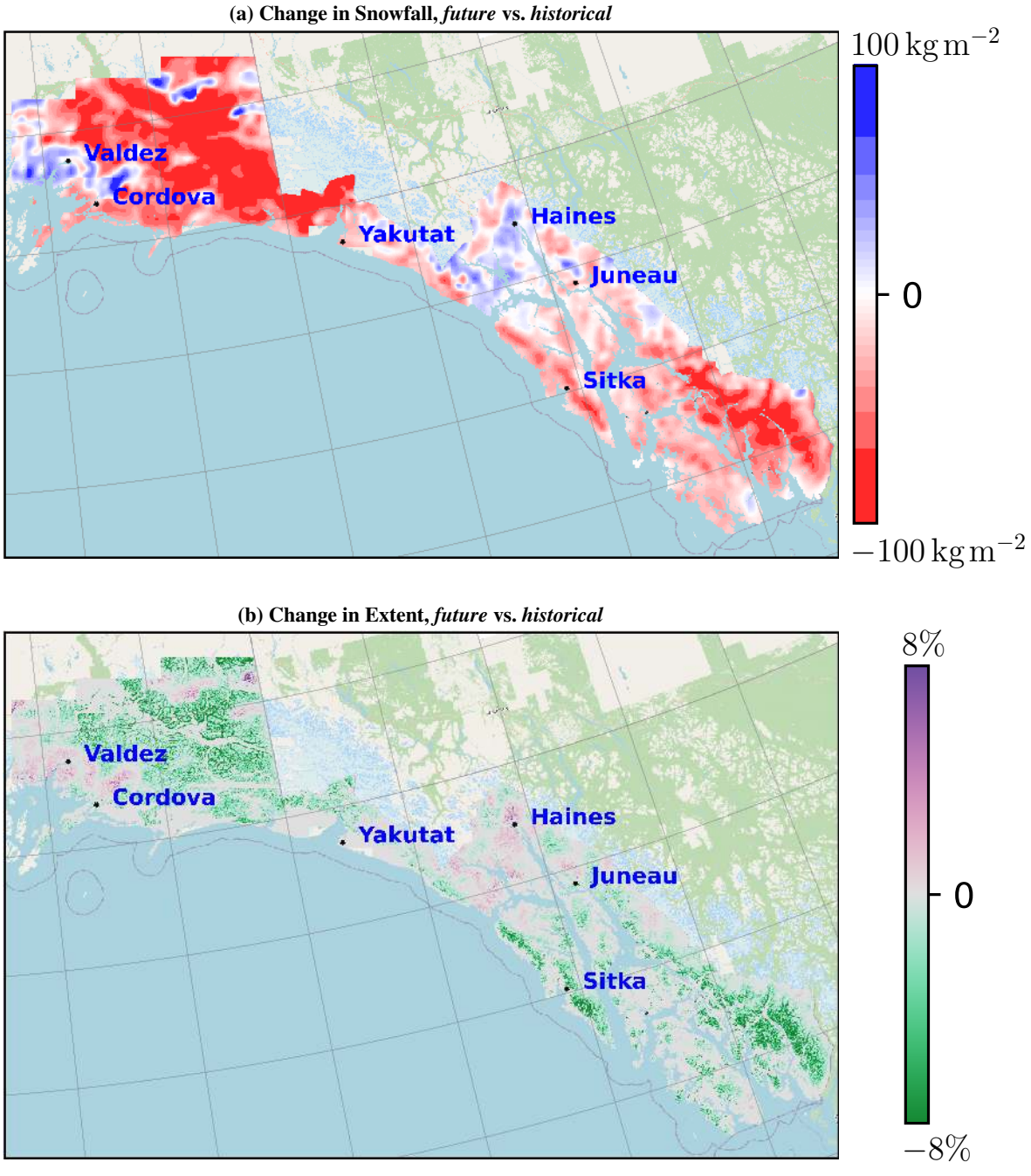

Figure 19. Changes in 3-day maximum snowfall (a) and avalanche risk (b) are plotted. Plot (b) shows change the portion of land at risk under *future* (2031-–2060) vs *historical* (1981–2010) scenarios for the *frequent* case, with negative numbers showing expected decreased future avalanche risk. The high spatial correlation between the two plots shows that expected precipitation changes are the primary driver of change in avalanche risk.

https://doi.org/10.5194/egusphere-2026-1345
Preprint. Discussion started: 18 March 2026

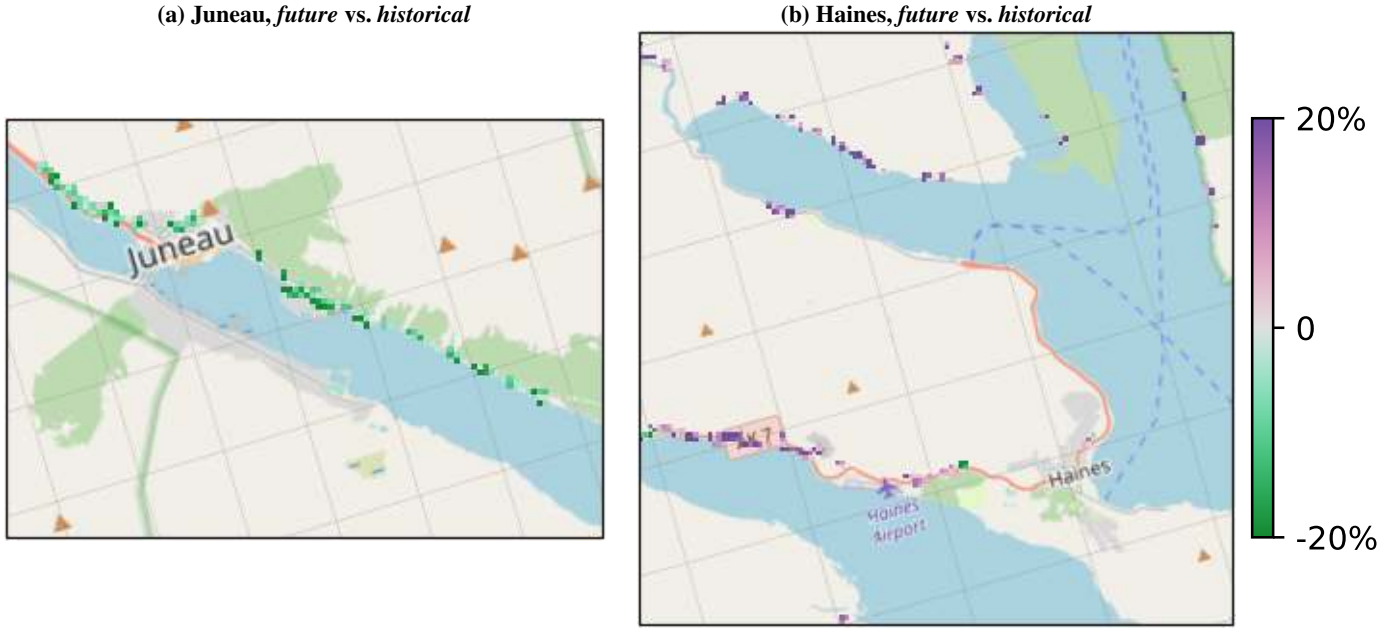

Figure 20. Expected changes in avalanche risk for Juneau and Haines at $100\,\mathrm{m} \times 100\,\mathrm{m}$ resolution for the *future* (2031-–2060) vs *historical* (1981–2010) scenarios. Grid cells with expected increased or decreased risk are plotted in purple and green respectively, whereas grid cells with no expected change are not plotted. Because the grid cells are $100\,\mathrm{m}$ on a side, a 10% reduction of risk within a call can be interpreted as an approximately $10\,\mathrm{m}$ retreat of maximal runout.

Low-elevation avalanche events, often arising in areas of complex vegetation, warrant focused investigation. Our study generated valuable data through the objective mapping of PRAs but the reliability of these PRAs, especially at lower elevations, depends on the accuracy of land cover maps. Unfortunately, the existing lack of quality vegetation coverage data makes this task difficult. Nevertheless, our findings show that low-elevation avalanches can make a difference in overall hazard susceptibility in certain areas. This is particularly true in Juneau, where the complex history of deforestation and regrowth complicates the assessment of how individual vegetation patches affect avalanche paths. This challenge, including the difficulty in accurately mapping PRAs due to poor forest data, helps explain the discrepancies found between this study and recent expert assessments on Behrends Avenue. It might be possible to partially overcome these problems using the methods of Sykes et al. (2022).

3.4 Recurrence Intervals and Extreme Value Theory

Uncertainty in defining recurrence intervals represents a core limitation of this and similar studies. Our hazard analysis is deterministic, meaning it models a single outcome for a given input event. This approach uses the common practice of estimating the size of the PRA and the return period of a single release volume (derived from 3-day maximum snowfall) to all possible hazard outcomes resulting from that volume. Considering the vast knowledge gap in Alaska, the uncertainties inherent in the data may overshadow any meaningful difference between high-resolution recurrence intervals (e.g., 10-, 30-, 100-, and 300-

https://doi.org/10.5194/egusphere-2026-1345
Preprint. Discussion started: 18 March 2026

year intervals). While future work would benefit from a systematic recurrence interval framework (El Rafei et al., 2023) or a probabilistic hazard analysis approach, a blunter, more qualitative approach to classifying areas as “more hazardous" or “less hazardous" aligns better with the currently available data.

Continued improvements in meteorological modeling will reduce uncertainty. The current $4\,\mathrm{km}$ WRF runs may not fully capture critical orographic effects. Better representation of orographic precipitation and downscaling would, in theory, improve results. Comparisons against finer resolution models in populated areas would help quantify the level of certainty. Both WRF and the downscaling model omit wind effects, which can significantly alter snow distribution. Properly modeling these effects at the spatial scale required for individual PRAs remains practically impossible with today’s state-of-the-art computational power.

Given that current downscaled products cannot resolve localized wind redistribution, our snow avalanche model forcing relies on the intensity of the snowfall events themselves. Specifically, the maximum 3-day snowfall values were calculated by averaging 30-year blocks of reanalysis and future climate data to isolate the single highest accumulation event for each period. This likely underestimates snowfall, especially for the 100-year and 300-year return intervals, because the maximum possible 3-day snowfall might not have occurred in the 30-year intervals. Although the use of Extreme Value Theory (Naveau et al., 2005) could allow for more accurate extrapolation to longer return periods, this might not matter in the face of other uncertainties.

While our findings suggest a regional decline in avalanche risk, these projections are constrained by the inherent limitations of climate modeling. Current models effectively capture macro-level trends in the frequency and intensity of extreme precipitation; however, they often lack the spatio-temporal resolution to resolve the localized, short-duration events typically associated with local disasters. This discrepancy between broad-scale accuracy and local-scale precision remains a significant challenge. Consequently, future hazard assessments must integrate in situ data with high-resolution modeling to bridge the gap between global climate patterns and site-specific impacts.

3.5 Assumptions and Limitations

While the methodology developed here provides a robust and scalable framework for large-scale avalanche susceptibility assessment, its implementation in a data-sparse environment necessitates the use of proxy datasets and modeling assumptions that introduce uncertainty throughout the workflow. The following limitations and assumptions must be considered when interpreting the results:

- **Constraints on Model Calibration and Validation:** A critical limitation in Alaska is the lack of a comprehensive avalanche incident database. Without a spatially and temporally extensive record of events, model calibration and tuning against well-documented avalanches is not possible in most places.
- **DEM Resolution and Terrain Representation:** High-resolution terrain data is central to the delineation of PRAs. Resampling to coarser resolutions (eg. $10\,\mathrm{m}$) for computational efficiency can smooth terrain features important for avalanche release.

https://doi.org/10.5194/egusphere-2026-1345
Preprint. Discussion started: 18 March 2026

- **Limitations of Climate and Snow Input Data:** Given Alaska's sparse meteorological observation network, this study employed climate reanalysis and downscaled projections to represent snowpack conditions. These substitutes add uncertainty, particularly for precipitation and snow depth, and restrict the validation of modeled release scenarios and return periods.

- **Limitations on Region-Specific Modeling:** The *SLF Standard Procedure* to compute release depth d_0, developed for the Swiss Alps, is not applicable to Southeast Alaska due to the lack of in situ data. Therefore, the *release depth* d_0 is set to the smoothed and downscaled *maximum 3-day snowfall* for the PRA, without any further corrections.

- **Deterministic Assumptions in PRA Modeling:** The methodology assumes that all delineated PRAs release deterministically under a prescribed maximum three-day snowfall scenario. Return periods are approximated through PRA size and simulated snow volume rather than through probabilistic models or historical avalanche frequency. While this simplification is necessary in data-poor regions, it departs from observed avalanche release variability and limits the realism of the outputs.

  Land Cover Data Accuracy and Interaction Limitations: The 2015 Alaska NLCD classification is used due to the absence of detailed vegetation data for determination of the forest mask. Errors in the that classification, particularly in forested regions, affect the correct identification of avalanche paths and in some cases exclude known tracks. Moreover, the RAMMS::LSHIM model handles vegetation interactions only in a limited way, omitting processes such as tree or debris entrainment. Built infrastructure is also not represented, even though it may significantly influence avalanche dynamics.

- **Model Scope and Phase Restrictions:** RAMMS::LSHIM is limited to simulating the dense-flow phase of dry-snow avalanches. It does not account for powder avalanches, wet-snow flows, multi-phase processes, entrainment effects, or the effects of snow temperature changes, narrowing its ability to capture complex avalanche behaviors in terrain prone to multiple avalanche types.

- **Unrepresented Initiation Mechanisms and Extreme Scenarios:** Some initiation triggers, such as cornice collapses, seismic activity, or events arising from extreme terrain features, are absent in the modeling framework. Likewise, low-frequency but large-scale avalanches in extensive alpine zones may be underrepresented, leading to potential underestimation of hazard runout or affected area.

4 Conclusions

This study presents the first systematic, high-resolution avalanche hazard indication maps for Southeast Alaska, representing a substantial advancement beyond prior qualitative or site-specific assessments. By combining downscaled reanalysis for historical baselines (1981–2010) with dynamically downscaled climate projections for mid-century conditions (2031–2060), we produced more than 3.5 million avalanche simulations that reveal a strongly heterogeneous spatial response of avalanche hazards

https://doi.org/10.5194/egusphere-2026-1345
Preprint. Discussion started: 18 March 2026

to projected climate change. While warming temperatures are associated with reduced hazard extents at lower elevations, increased atmospheric moisture is projected to enhance potential runout in select high-elevation areas by mid-century. Although avalanche modeling in data-sparse regions is subject to climatic uncertainty and scale-dependent bias, the framework presented here provides an immediately useful basis for hazard-informed infrastructure planning and land-use decision-making. By explicitly linking historical and future climate conditions within a consistent modeling approach, this work supports the evaluation of evolving hazard patterns under ongoing climate change. The resulting maps establish a defensible regional baseline and a transferable methodological foundation upon which future probabilistic avalanche hazard assessments can be developed for Southeast Alaska and other sub-Arctic mountain environments.

https://doi.org/10.5194/egusphere-2026-1345
Preprint. Discussion started: 18 March 2026

References

Bartelt, P. and Stöckli, V.: The Influence of Tree and Branch Fracture, Overturning and Debris Entrainment on Snow Avalanche Flow, Annals of Glaciology, 32, 209–216, https://doi.org/10.3189/172756401781819544, 2001.

Bebi, P., Bast, A., Helzel, K., Schmucki, G., Brozova, N., and Bühler, Y.: Avalanche protection forest: From process knowledge to interactive maps, in: Protective forests as ecosystem-based solution for disaster risk reduction (Eco-DRR), IntechOpen, https://doi.org/10.5772/intechopen.99514, 2021.

Blaschke, T.: Object based image analysis for remote sensing, ISPRS journal of photogrammetry and remote sensing, 65, 2–16, https://doi.org/10.1016/j.isprsjprs.2009.06.004, 2010.

Boensch, M., Rudolf-Miklau, F., Sauermoser, S., and Mears, A.: The technical avalanche protection handbook, John Wiley & Sons, https://doi.org/10.1002/9783433603840, 2014.

Bühler, Y.: Automated Snow Avalanche Release Area Delineation - Validation of Existing Algorithms and Proposition of a New Object-Based Approach for Large Scale Hazard Indication Mapping, Natural Hazards and Earth System Sciences, https://doi.org/10.5194/nhess-18-3235-2018, 2018.

Buhler, Y. and Kuhne, R.: Linking Modelled Potential Release Areas with Avalanche Dynamic Simulations: An Automated Approach for Efficient Avalanche Hazard Indication Mapping, in: International Snow Science Workshop Proceedings, Innsbruck, Austria, 2018.

Bühler, Y., Kumar, S., Veitinger, J., Christen, M., Stoffel, A., and Snehmani: Automated Identification of Potential Snow Avalanche Release Areas Based on Digital Elevation Models, Natural Hazards and Earth System Sciences, 13, 1321–1335, https://doi.org/10.5194/nhess-13-1321-2013, 2013.

Bühler, Y., Bebi, P., Christen, M., Margreth, S., Stoffel, L., Stoffel, A., Marty, C., Schmucki, G., Caviezel, A., Kühne, R., Wohlwend, S., and Bartelt, P.: Automated Avalanche Hazard Indication Mapping on a Statewide Scale, Natural Hazards and Earth System Sciences, 22, 1825–1843, https://doi.org/10.5194/nhess-22-1825-2022, 2022.

Carswell Jr., W. J.: The 3D Elevation Program: Summary for Alaska, Report 2013-3083, US Geological Survey, Reston, VA, https://doi.org/10.3133/fs20133083, 2013.

Christen, M., Kowalski, J., and Bartelt, P.: RAMMS: Numerical Simulation of Dense Snow Avalanches in Three-Dimensional Terrain, Cold Regions Science and Technology, 63, 1–14, https://doi.org/10.1016/j.coldregions.2010.04.005, 2010.

Dickson, I.: How a Juneau Subdivision Came to Be at 'Unacceptable' Risk for a Destructive Avalanche, Alaska Public Media PBS / NPR: KTOO, 2021.

Duhamel, P.: Fast Fourier Transforms: A Tutorial Review and a State of the Art, Signal Processing, 19, 259–299, https://doi.org/10.1016/0165-1684(90)90158-U, 1990.

El Rafei, M., Sherwood, S., Evans, J., Dowdy, A., and Ji, F.: Biases in Estimating Long-Term Recurrence Intervals of Extreme Events Due To Regionalized Sampling, Geophysical Research Letters, 50, e2023GL105 286, https://doi.org/10.1029/2023GL105286, 2023.

Fesler, D. and Fredson, J.: Avalanche Hazard Evaluation & Mitigation Recommendations for the Town Mountain and Duck Flats Avalanche Areas, Valdez, Alaska, Tech. rep., Alaska Mountain Safety Center, Anchorage, AK, 2000.

Fischer, J.-T., Kowalski, J., and Pudasaini, S. P.: Topographic Curvature Effects in Applied Avalanche Modeling, Cold Regions Science and Technology, 74–75, 21–30, https://doi.org/10.1016/j.coldregions.2012.01.005, 2012.

Freeman, H. and Shapira, R.: Determining the Minimum-Area Encasing Rectangle for an Arbitrary Closed Curve, Communications of the ACM, 18, 409–413, https://doi.org/10.1145/360881.360919, 1975.

https://doi.org/10.5194/egusphere-2026-1345
Preprint. Discussion started: 18 March 2026

GDAL/OGR contributors: GDAL/OGR Geospatial Data Abstraction software Library, Open Source Geospatial Foundation, https://doi.org/10.5281/zenodo.5884351, 2024.

Gent, P. R., Danabasoglu, G., Donner, L. J., Holland, M. M., Hunke, E. C., Jayne, S. R., Lawrence, D. M., Neale, R. B., Rasch, P. J., Vertenstein, M., Worley, P. H., Yang, Z.-L., and Zhang, M.: The Community Climate System Model Version 4, Journal of Climate, 24, 4973–4991, https://doi.org/10.1175/2011JCLI4083.1, 2011.

Getreuer, P.: A Survey of Gaussian Convolution Algorithms, Image Processing On Line, 3, 286–310, https://doi.org/10.5201/ipol.2013.87, 2013.

Hackett, S. and Santeford, H.: Avalanche Zoning in Alaska, U.S.A., Journal of Glaciology, 26, https://doi.org/10.3189/S0022143000010911, 1980.

Harris, A. and Farr, W.: The Forest Ecosystem of Southeast Alaska: Forest Ecology and Timber Management, Tech. Rep. PNW-25, USDA Forest Service, 1974.

Harvey, S., Schmudlach, G., Buhler, Y., Durr, L., Stoffel, A., and Christen, M.: Avalanche Terrain Maps for Backcountry Skiing in Switzerland, in: Proceedings ISSW, pp. 1625–1631, Innsbruck, Austria, 2018.

Issler, D., Gisnås, K. G., Gauer, P., Glimsdal, S., Domaas, U., and Sverdrup-Thygeson, K.: Naksin–A new approach to snow avalanche hazard indication mapping in Norway, Available at SSRN 4530311, https://doi.org/10.2139/ssrn.4530311, 2023.

Jin, S., Homer, C., Yang, L., Danielson, P., Dewitz, J., Li, C., Zhu, Z., Xian, G., and Howard, D.: Overall Methodology Design for the United States National Land Cover Database 2016 Products, Remote Sensing, 11, 2971, https://doi.org/10.3390/rs11242971, 2019.

Lader, R., Bidlack, A., Walsh, J. E., Bhatt, U. S., and Bieniek, P. A.: Dynamical Downscaling for Southeast Alaska: Historical Climate and Future Projections, Journal of Applied Meteorology and Climatology, 59, 1607–1623, https://doi.org/10.1175/JAMC-D-20-0076.1, 2020.

Lader, R., Bhatt, U. S., Walsh, J. E., and Bieniek, P. A.: Projections of Hydroclimatic Extremes in Southeast Alaska under the RCP8.5 Scenario, Earth Interactions, 26, 180–194, https://doi.org/10.1175/EI-D-21-0023.1, 2022.

Littell, J. S., McAfee, S. A., and Hayward, G. D.: Alaska Snowpack Response to Climate Change: Statewide Snowfall Equivalent and Snowpack Water Scenarios, Water, 10, 668, https://doi.org/10.3390/w10050668, 2018.

Maggioni, M. and Gruber, U.: The influence of topographic parameters on avalanche release dimension and frequency, Cold Regions Science and Technology, 37, 407–419, https://doi.org/10.1016/S0165-232X(03)00080-6, 2003.

Margreth, S. and Romang, H.: Effectiveness of mitigation measures against natural hazards, Cold Regions Science and Technology, 64, 199–207, https://doi.org/10.1016/j.coldregions.2010.04.013, 2010.

Mears, A., Mears, A., Colorado, G., Fesler, D., and Fredson, J.: Juneau Area Mass-Wasting & Snow Avalanche Hazard Analysis, Tech. rep., City and Borough of Juneau, 1992.

Meinshausen, M., Smith, S. J., Calvin, K., Daniel, J. S., Kainuma, M. L., Lamarque, J.-F., Matsumoto, K., Montzka, S. A., Raper, S. C., Riahi, K., et al.: The RCP greenhouse gas concentrations and their extensions from 1765 to 2300, Climatic change, 109, 213, https://doi.org/10.1007/s10584-011-0156-z, 2011.

Naveau, P., Nogaj, M., Ammann, C., Yiou, P., Cooley, D., and Jomelli, V.: Statistical Methods for the Analysis of Climate Extremes, Comptes Rendus. Géoscience, 337, 1013–1022, https://doi.org/10.1016/j.crte.2005.04.015, 2005.

Peitzsch, E. H., Pederson, G., Martin, J., Hood, E., Greene, E., Birkeland, K. E., Wolken, G., Kichas, N., Stahle, D., and Harley, J. R.: Big avalanches in a changing climate: Using tree-ring derived avalanche chronologies to examine avalanche frequency across multiple climate types, in: Proceedings, International Snow Science Workshop 2023, pp. 547–553, Montana State University Library, Bend, OR, 2023.

https://doi.org/10.5194/egusphere-2026-1345
Preprint. Discussion started: 18 March 2026

Qin, Y., Ren, G., Zhai, T., Zhang, P., and Wen, K.: A New Methodology for Estimating the Surface Temperature Lapse Rate Based on Grid Data and Its Application in China, Remote Sensing, 10, 1617, https://doi.org/10.3390/rs10101617, 2018.

Riahi, K., Rao, S., Krey, V., Cho, C., Chirkov, V., Fischer, G., Kindermann, G., Nakicenovic, N., and Rafaj, P.: RCP 8.5—A scenario of comparatively high greenhouse gas emissions, Climatic change, 109, 33, https://doi.org/10.1007/s10584-011-0149-y, 2011.

Rudolf-Miklau, F., Sauermoser, S., and Mears, A. I.: The Technical Avalanche Protection Handbook, Wiley Online Library, https://doi.org/10.1002/9783433603840.ch01, 2014.

Saha, S., Moorthi, S., Pan, H.-L., Wu, X., Wang, J., Nadiga, S., Tripp, P., Kistler, R., Woollen, J., Behringer, D., Liu, H., Stokes, D., Grumbine, R., Gayno, G., Wang, J., Hou, Y.-T., Chuang, H.-y., Juang, H.-M. H., Sela, J., Iredell, M., Treadon, R., Kleist, D., Van Delst, P., Keyser, D., Derber, J., Ek, M., Meng, J., Wei, H., Yang, R., Lord, S., Van Den Dool, H., Kumar, A., Wang, W., Long, C., Chelliah, M., Xue, Y., Huang, B., Schemm, J.-K., Ebisuzaki, W., Lin, R., Xie, P., Chen, M., Zhou, S., Higgins, W., Zou, C.-Z., Liu, Q., Chen, Y., Han, Y., Cucurull, L., Reynolds, R. W., Rutledge, G., and Goldberg, M.: The NCEP Climate Forecast System Reanalysis, Bulletin of the American Meteorological Society, 91, 1015–1058, https://doi.org/10.1175/2010BAMS3001.1, 2010.

Sappington, J. M., Longshore, K. M., and Thompson, D. B.: Quantifying landscape ruggedness for animal habitat analysis: a case study using bighorn sheep in the Mojave Desert, The Journal of wildlife management, 71, 1419–1426, https://doi.org/10.2193/2005-723, 2007.

Schmudlach, G. and Köhler, J.: Automated avalanche risk rating of backcountry ski routes, in: Proceedings ISSW, pp. 450–456, 2016.

Skamarock, W. C., Klemp, J. B., Dudhia, J., Gill, D. O., Barker, D. M., Duda, M. G., Huang, X.-Y., Wang, W., and Powers, J. G.: A Description of the Advanced Research WRF Version 4, Tech. rep., NCAR, Boulder, CO, 2019.

Sobel, I.: An Isotropic 3x3 Image Gradient Operator, Presentation at Stanford A.I. Project 1968, 2014.

Sykes, J., Haegeli, P., and Bühler, Y.: Automated snow avalanche release area delineation in data-sparse, remote, and forested regions, Natural Hazards and Earth System Sciences, 22, 3247–3270, https://doi.org/10.5194/nhess-22-3247-2022, 2022.

TetraTech: Downtown Juneau Landslide and Avalanche Hazard Assessment, Tech. Rep. ENG.EARC03168-01, City and Borough of Juneau, Juneau, Alaska, 2022.

Van Vuuren, D. P., Edmonds, J., Kainuma, M., Riahi, K., Thomson, A., Hibbard, K., Hurtt, G. C., Kram, T., Krey, V., Lamarque, J.-F., et al.: The representative concentration pathways: an overview, Climatic change, 109, 5, https://doi.org/DOI 10.1007/s10584-011-0148-z, 2011.

Védrine, L., Li, X., and Gaume, J.: Detrainment and Braking of Snow Avalanches Interacting with Forests, Natural Hazards and Earth System Sciences, 22, 1015–1028, https://doi.org/10.5194/nhess-22-1015-2022, 2022.

Viglietti, D., Letey, S., Motta, R., Maggioni, M., and Freppaz, M.: Snow and Avalanche: The Influence of Forest on Snowpack Stability, in: Proceedings ISSW, 2009.

White, K. S., Hood, E., Wolken, G. J., Peitzsch, E. H., Bühler, Y., Wikstrom Jones, K., and Darimont, C. T.: Snow avalanches are a primary climate-linked driver of mountain ungulate populations, Communications Biology, 7, 423, https://doi.org/10.1038/s42003-024-06073-0, 2024.

Wolken, G., Fischer, E., Hendricks, M., and Wikstrom, J.: Alaska Snow Avalanche Hazard Database, Tech. rep., Alaska Division of Geological & Geophysical Surveys, https://doi.org/10.14509/32076, 2026.

Wooley, C.: The Myth of the "Pristine Environment": Past Human Impacts in Prince William Sound and the Northern Gulf of Alaska, Spill Science & Technology Bulletin, 7, 89–104, https://doi.org/10.1016/S1353-2561(02)00063-4, 2002.

WSL Institute: Avalanche Mitigation Study: Behrends Avenue Avalanche Path and White Subdivision Avalanche Path, Juneau, Alaska, Tech. Rep. G2011.21, WSL Institute for Snow and Avalance Research SLF, 2011.

https://doi.org/10.5194/egusphere-2026-1345
Preprint. Discussion started: 18 March 2026

Zhu, D., Ren, Q., Xuan, Y., Chen, Y., and Cluckie, I. D.: An Effective Depression Filling Algorithm for DEM-based 2-D Surface Flow Modelling, Hydrology and Earth System Sciences, 17, 495–505, https://doi.org/10.5194/hess-17-495-2013, 2013.

Code Availability

This study relied on code with multiple different authors under multiple licenses. Public domain portions are available online via https://github.com/AlaskaLargeScaleSnowAvalanche/akramms/tree/260312-Submission. RAMMS may be licensed at https://ramms.ch/shop/. Additionally, running these codes requires at least one comptuer running Linux, one running Microsoft Windows, and licenses for the commercial products ArCGIS, eCognition and IDL.

Data Availability

The results of this study are available online via Wolken et al. (2026).

Competing Interests

Author Marc Christen is the founder of RAMMS, AG. Author Yves Bühler is an Editor at NHESS.

Acknowledgements

Funding for this work was provided by the Alaska Climate Adaptation Science Center, a cooperative agreement between the U.S. Geological Survey and the University of Alaska Fairbanks. Thank you to Tobias Schworer for his careful internal review.